ANL/CSE-13/16

Sorbent Selection Progress Report

Chemical Science and Engineering Division

About Argonne National Laboratory

Argonne is a U.S. Department of Energy laboratory managed by UChicago Argonne, LLC under contract DE-AC02-06CH11357. The Laboratory's main facility is outside Chicago, at 9700 South Cass Avenue, Argonne, Illinois 60439. For information about Argonne and its pioneering science and technology programs, see www.anl.gov.

Availability of This Report

This report is available, at no cost, at http://www.osti.gov/bridge. It is also available on paper to the U.S. Department of Energy and its contractors, for a processing fee, from:

U.S. Department of Energy
Office of Scientific and Technical Information
P.O. Box 62
Oak Ridge, TN 37831-0062
phone (865) 576-8401
fax (865) 576-5728
reports@adonis.osti.gov

Disclaimer

This report was prepared as an account of work sponsored by an agency of the United States Government. Neither the United States Government nor any agency thereof, nor UChicago Argonne, LLC, nor any of their employees or officers, makes any warranty, express or implied, or assumes any legal liability or responsibility for the accuracy, completeness, or usefulness of any information, apparatus, product, or process disclosed, or represents that its use would not infringe privately owned rights. Reference herein to any specific commercial product, process, or service by trade name, trademark, manufacturer, or otherwise, does not necessarily constitute or imply its endorsement, recommendation, or favoring by the United States Government or any agency thereof. The views and opinions of document authors expressed herein do not necessarily state or reflect those of the United States Government or any agency thereof, Argonne National Laboratory, or UChicago Argonne, LLC.

ANL/CSE-13/16

Sorbent Selection Progress Report

by
Dominique Stepinski[1], Amanda Ziegler[1], Jim Jerden[1], Jeff Fortner[1], Kevin Quigley[1], Carol Mertz[1], Art Guelis[1], Sergey Chemerisov[1], Yifan Tsai[1], Allen Bakel[1], George Vandegrift[1], Pei Chun[2], and Linda Wang[2]
[1]Chemical Science and Engineering Division, Argonne National Laboratory
[2]Purdue University

prepared for
U.S. Department of Energy, National Nuclear Security Administration,
Office of Defense Nuclear Nonproliferation

July 24, 2009

CONTENTS

1 INTRODUCTION 1

1.1 Overview 1
1.2 Summary of Sorbents 1

2 PHYSICAL PROPERTIES OF SORBENTS 3

2.1 Introduction 3
2.2 Methods and Results 3
2.3 Conclusions 9

3 UPTAKE OF Mo FROM URANYL NITRATE SOLUTIONS 10

3.1 Experiment 10
3.1.1 Preparation of Uranium Solutions 10
3.1.2 Preparation of ^{99}Mo Spike Solution 11
3.1.3 Batch Uptake Measurements 11
3.1.4 Counting of ^{99}Mo 11

4 LANGMUIR ISOTHERMS 12

5 CHEMICAL STABILITY 17

5.1 Sorbent Stability to pH 1 and 14 Washing Cycles 17
5.2 Discoloration of Mo Solution 17
5.3 Solubility of TiO_2 20
5.4 Experiments of Sorbent Leaching during Uptake of Competing Components 22
5.5 Decrease of Column Void Fractions 22

6 RADIOLYTIC STABILITY 23

7 URANIUM RECOVERY 24

7.1 Batch Studies 24
7.2 Column Studies 24
7.3 Experiment 25

8 X-RAY DIFFRACTION ANALYSIS OF SORBENT RESIDUE 27

9 DYNAMIC LIGHT SCATTERING ANALYSIS OF T52 AND T5M AQUEOUS SUSPENTIONS 29

9.1 Introduction 29

CONTENTS (Cont.)

9.2 Conclusions 29
9.3 Experiment 36

10 ALUMINA SOLUBILITY 37

11 Mo STRIPPING 40

11.1 Introduction 40
11.2 Experiment 41

12 UPTAKE OF COMPETING COMPONENTS 42

13 COLUMN SIZE 43

14 FUTURE WORK 44

14.1 Langmuir Isotherm Data in the Presence of 150 g-U/L, pH 1, 60°C 44
14.2 Presence of Nanoparticles in the Reactor Solution 44
14.3 Mechanical Stability of the Sorbents 44
14.4 Aluminum Hydroxide 44
14.5 Washing of Uranyl Nitrate from S80 Packed Column 44
14.6 Mo Recovery 45

15 REFERENCES 46

FIGURES

1 Observed BET Surface Area Measurements 5

2 Measured XRD for T5M-Type and T52-Type Sorbent Materials from the Batches Received in 2008 6

3 Measured XRD for T5M-Type and T52-Type Sorbent Materials Comparing Recent Batches with Representative Older Batches 7

4 Comparison of T52 and Rutile 8

5 Comparison of T5M and Anatase 8

6 Comparison of S80 and Anatase 9

FIGURES (Cont.)

7 Uptake of 0.5 ppm Mo from a Uranyl Nitrate Solution at pH 1 and 60°C by Sorbents Being Considered for MIPS 10

8 Combined Results of Langmuir Isotherm Data 15

9 Scanning Electron Microscope Image of Mo Precipitated Layer on the Surface of T5M Sorbent 16

10 Sorbent Stability after Exposure to pH 1 and pH 14 Washing Cycles 18

11 Speciation Diagram for Titania Anatase Modification at 25°C 20

12 Speciation Diagram for Titania Rutile Modification at 25°C 21

13 Uptake of Mo as a Function of Uranyl Nitrate Concentration at pH 1 and 25°C, 55°C, and 85°C for Batches of T52 and T5M 21

14 Effect of Radiation Dose on Uptake of Mo 23

15 Uptake of Tracer Levels of U-233 from HNO_3 Solutions 25

16 Elution of Uranium from T5M, T52, S80, and AG4 26

17 Comparison of X-ray Diffraction from the Precipitate with That Obtained from a Blank Sample Holder and the T5M and T52 Sorbents 28

18 X-ray Diffraction Detail 28

19 Monomodal Size Distribution for T52, First Wash 30

20 Correlation Function for T52, First Wash 30

21 Multisize Distribution for T52, First Wash 31

22 Monomodal Size Distribution for T52, Second Wash 31

23 Correlation Function for T52, Second Wash 32

24 Multisize Distribution for T52, Second Wash 32

25 Monomodal Size Distribution for T5M, First Wash 33

26 Correlation Function for T5M, First Wash 33

FIGURES (Cont.)

27 Multisize Distribution for T5M, First Wash 34

28 Monomodal Size Distribution for T5M, Second Wash 34

29 Correlation Function for T5M, Second Wash..... 35

30 Multisize Distribution for T5M, Second Wash..... 35

31 Solubility of Alumina as Function of pH Modeled by Using OLI-ESP Code..... 37

32 Solubility Profiles 38

33 Images of Alumina Sample Act. I from Sigma Aldrich, 150 Mesh 39

34 Images of Alumina Sample AG4 from BioRad, 150 Mesh 39

35 Percent Recovery of Mo-99 as a Function of the Number of Bed Volumes 40

TABLES

1 BET Surface Area Determination of Sorbents..... 4

2 Langmuir Isotherm Data Acquired by Equilibrating 10 mL of Solution Containing 1.9 M $NaNO_3$, 0.1 M HNO_3, and Na_2MoO_4 at Various pHs with Sorbent 13

3 Langmuir Isotherm Data Acquired by Equilibrating 10 mL of Solution Containing 2 M $NaNO_3$, 0.09 M HNO_3, and Na_2MoO_4 at a pH of 1 with Sorbent 13

4 Langmuir Isotherm Data Acquired by Equilibrating 1 mL of Solution Containing 1.3 M $NaNO_3$, 0.1 M HNO_3, and Na_2MoO_4 at a pH of 1 with Sorbent 14

5 Langmuir Isotherm Data Acquired by Equilibrating 1 mL of Solution Containing 1.3 M $NaNO_3$, 0.1 M HNO_3, and Na_2MoO_4 at a pH of 1 with Sorbent 15

6 Composition of 0.1 M HNO_3 and Mo Solutions after Contact with Sorbents..... 18

7 Uptake of Tracer Levels of U-233 from HNO_3 Solutions 25

TABLES (Cont.)

8 Recovery of Uranyl Nitrate from T5M, T52, S80, and AG4 26

9 Summary of Dynamic Light Scattering Results for T52 and T5M Samples 29

10 ICP-MS Results of Alumina Solubility in 0.1 M HNO_3 38

11 Percent Recovery of Mo-99 from T5M, T52, S80, and AG4 40

12 Uptake of Ions from a Simulated Fuel Solution in the Absence of Uranium 42

13 Recommended Column Designs Based on Pressure Drop Constraints and Mass Transfer Zone Calculations 43

SORBENT SELECTION PROGRESS REPORT

1 INTRODUCTION

1.1 OVERVIEW

Argonne National Laboratory is currently helping Babcock and Wilcox (B&W) develop a process for recovering ^{99}Mo from the low enriched uranium (LEU) fuel solution of an aqueous homogeneous reactor (AHR). To recover ^{99}Mo from a concentrated uranium solution, we are evaluating six sorbents: (1 and 2) T52 (25 mol% SnO_2 and 75 mol% TiO_2) and T5M (5 mol% ZrO_2 and 95 mol% TiO_2), both of which are manufactured by Termoxid Scientific and Production Company, Zarechnyi, Russia; (3) AG4 alumina manufactured by BioRad; (4) Sachtopore-80 (TiO_2) from ZirChrom Separations; and (5 and 6) 200- and 500-µm Adsorbsia sorbents from Dow Chemical.

This report describes batch studies comparing the uptake of ^{99}Mo from uranium solutions, chemical and radiolytic stability, and sorbent physical properties. The uranyl nitrate concentration being considered for AHR operation is 150 g-U/L at a pH 1.

1.2 SUMMARY OF SORBENTS

T52 is a nanocrystalline version of rutile that is predicted to be more chemically stable than T5M (anatase). Our experimental studies confirmed these findings and show that T52 has lower solubility in nitric acid and that its K_d values do not decrease when sorption is carried out at elevated temperatures. In the presence of uranium, T52 also has Mo K_d values that are higher than those of T5M. T52 has uranium K_d values that are 10 times lower than those of T5M. As a result, a T5M-packed column retains a significant quantity of uranium and requires scrubbing with a larger amount of 0.1 M HNO_3 than does a T52-packed column.

Both the T52 and T5M sorbent materials are composed of nanoparticles; vigorous shaking of these particle suspensions can dislodge nanoparticles from them. The bulk of the dislodged nanoparticles from the T52 sorbent can be removed by using a 1-µm filter, whereas the nanoparticle aqueous suspension from the T5M sorbent requires a 0.2-µm filter. The formation of nanoparticles in the sorbent materials is probably a result of sorbent mechanical degradation and will be studied further.

S80 is a nanocrystalline version of rutile, and its chemical stability is comparable to that of T52, probably because of its particle uniformity. In the presence of uranium, S80 has Mo K_d values that are higher than those of T5M and T52. However, S80 retains uranium with a significant distribution ratio, and it requires scrubbing with 20–30 bed volumes of 0.1 M HNO_3 or with a smaller volume of 1 M HNO_3 to completely remove uranium from the column. Scrubbing an S80-packed column with 1 M HNO_3 leads to a loss of 1.5% Mo (batch experiment,

24 h, 60°C) and might lead to corrosion of the recovery system and accelerated sorbent degradation.

Alumina, in the presence of 150 g-U/L, has Mo K_d values that are two orders of magnitude lower than those of the titania-based sorbents (K_d ~270). It remains to be shown whether a column with MIPS requirements can be designed under those conditions. Uranium uptake by alumina is low (K_d ~10), and an alumina-packed column does not retain significant amounts of uranium during the loading cycle. Alumina has a relatively high solubility in 0.1 M HNO_3. The amount of aluminum present in the solution after 24 hours of contact with 0.1 M HNO_3 is about 200 parts per million (ppm). For comparison, a 24-h contact of T52 and S80 with 0.1 M HNO_3 results in a titanium hydroxide concentration of about 200 parts per billion (ppb). The implications for the presence of a high concentration of aluminum ion in the fuel solution need to be determined.

Adsorbsia sorbents degraded and formed a fine powder after contact with 0.1 M HNO_3 (3 h) and 1 M NaOH (1 h) at 60°C. Therefore, they will not be a suitable sorbent for the MIPS.

Based on preliminary results, T52, T5M, and S80 are quite selective for Mo(VI) over other fission products and uranium. However, the K_d values for S80 for several fission products and uranium are high enough to require significant volumes of wash solution following column loading. Given what is known at this time, a down select based on Kd values and stability would leave only two sorbents (T52 and S80) for further study. T52 appears to have a slight edge over S80.

2 PHYSICAL PROPERTIES OF SORBENTS

2.1 INTRODUCTION

T52 and T5M were examined by surface area determination and x-ray diffraction (XRD). The objective was to determine whether uncontrolled variations in these properties among batches might be responsible for variable performance in ^{99}Mo separations (Vandegrift et al. 2008). Original specimens provided were labeled Radsorb Lot 2002-002, Radsorb Lot 6, Radsorb Lot 4, Termoxid-52M (T52-type), Isosorb Lot 5, Isosorb Lot 2002-001, and Termoxid-5M (T5M-type). These were analyzed, and the results were reported on in March 2008 (Fortner 2008). Subsequently, new batches of sorbent were provided, labeled $T5M_1$, $T5M_2$, $T5M_3$, $T5M_4$, $T52_1$, $T52_2$, $T52_3$, and $T52_4$. For simplicity, we will use "T5M-1" in place of "$T5M_1$," etc., in further discussion and figures.

2.2 METHODS AND RESULTS

Surface area measurements were obtained by adsorption isotherm measurements using the Brunauer, Emmett, and Teller (BET) method (Brunauer et al. 1938). The BET analysis used nitrogen (N_2) as the adsorbed gas, with five-point isotherms fitted to the form

$$\frac{P}{P_0} = a + b\left[V_A\left(P_0/P - 1\right)\right]^{-1},$$

where P/P_0 was the relative pressure, V_A was the volume of N_2 adsorbed (at standard temperature and pressure, STP), and the parameters a and b were related to the adsorption energy and monolayer surface area. All fits had a linear correlation coefficient of better than 99.9%. The measured values appear in Table 1 and Figure 1. Also appearing in Table 1 are determinations of geometric surface area for selected specimens obtained by using electron microscopy (Beasley 2007). Note that the BET surface area exceeded the geometric surface area (the apparent surface area of the roughly spherical particles) by about 5.5 orders of magnitude. Such large BET surface areas are characteristic of nanostructured materials, such as those used in catalysis or for chemical separations.

Prior to measuring BET surface area, we had to de-gas the sorbent material under vacuum at an elevated temperature (150°C). The vacuum heat treatment in each case caused the material to darken — from amber (T52-type) or light yellow (T5M-type) — to dark brown. After exposure to air after the measurements, the samples returned to their original color within a few hours. Nonetheless, there remained some concern that the BET measurements might have affected the microstructure of the sorbents, so samples of the vacuum heat-treated material were analyzed by XRD along with pristine samples. No changes in XRD with the heat treatment were observed (see discussion that follows).

TABLE 1 BET Surface Area Determination of Sorbents[a]

Sorbent	Type	BET Surface Area (m^2/g)	Projected Area per Particle (cm^2)[b]	Geometric Surface Area (m^2/g)[b]	BET/Geometric Surface Area
Radsorb Lot 2002-002	T52	92.3			
Radsorb Lot 6	T52	89.6			
Radsorb Lot 4	T52	84.8			
Termoxid-52M	T52	95.5	0.0043	0.0021	45,700
T52-1	T52	90.0			
T52-2	T52	100.2			
T52-3	T52	84.7			
T52-4	T52	88.0			
Isosorb Lot 5	T5M	141.0			
Isosorb Lot 2002-001	T5M	153.8			
Termoxid-5M	T5M	151.9	0.0036	0.0023	66,500
T5M-1	T5M	142.4			
T5M-2	T5M	139.6			
T5M-3	T5M	146.8			
T5M-4	T5M	142.9			
S80[c]	60A	100			

[a] Some of these data are reported on in Fortner (2008).

[b] Based on data in Beasley (2007).

[c] Based on data in Winkler et al. (1999).

XRD was measured by using the Kα line of copper (wavelength of 0.15406 nm) in a diffractometer. To obtain proper instrument resolution of the diffraction lines, the samples had to be crushed to a fine powder so that they could be evenly dispersed on the diffractometer sample plate. Measurements were made on the as-received material after it was crushed to a fine powder. A previous report on older batches of T5M and T52 also showed no observed changes induced in the XRD patterns from de-gassing under vacuum at 150°C during the BET measurements (Fortner 2008). The XRD data for both the T5M- and T52-type specimens showed significant diffraction peak broadening (characteristic of small scattering domain sizes). The XRD peak widths of both sorbent types indicated crystal domain sizes between 9 and 11 nm. As Figure 2 illustrates, the data indicated remarkable reproducibility among the sorbent batches for each type.

Figure 3 compares representative XRD patterns from a new batch to those obtained from an older batch (reported on in Fortner 2008). There were no significant differences for the T5 material, aside from a reduced intensity of small angle scattering, which may not be quantitative owing to the geometry of the diffractometer. An interesting point is that the newer batch of T52 appeared to have somewhat broader diffraction peaks, suggesting smaller crystalline domains than those in the older batch(es). As seen in Figure 1, however, this effect had no impact on the BET measurements. It is possible that the additional XRD peak broadening

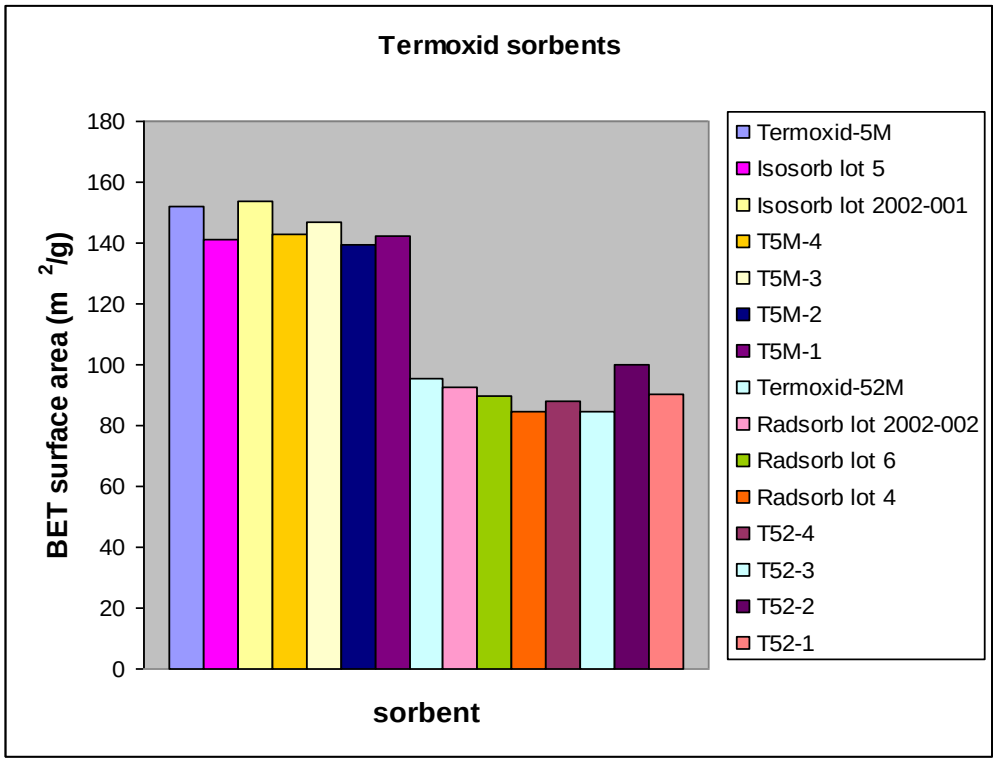

FIGURE 1 Observed BET Surface Area Measurements (The variation among the T5M- and T52-types was relatively small.)

seen in the T52 specimens was due to nonuniform internal stress, or (more likely), it could have been an artifact of the differences in the setup of the apparatus between measurements.

Figures 4, 5, and 6 compare the sorbent diffraction patterns with two different crystal structures of TiO_2, rutile and anatase, from the JCPDS-ICDD (Joint Committee on Powder Diffraction Standards, International Center for Diffraction Data) database. In these figures, the diffraction data are plotted as d-spacings, which are related to the diffraction angle by the Bragg relation

$$n\lambda = 2d \sin\theta,$$

where n, the order of the diffraction, is taken to be 1 for the conversion. From these plots, it is apparent that T52 is a nanocrystalline version of rutile and that T5M and S80 are nanocrystalline versions of anatase.

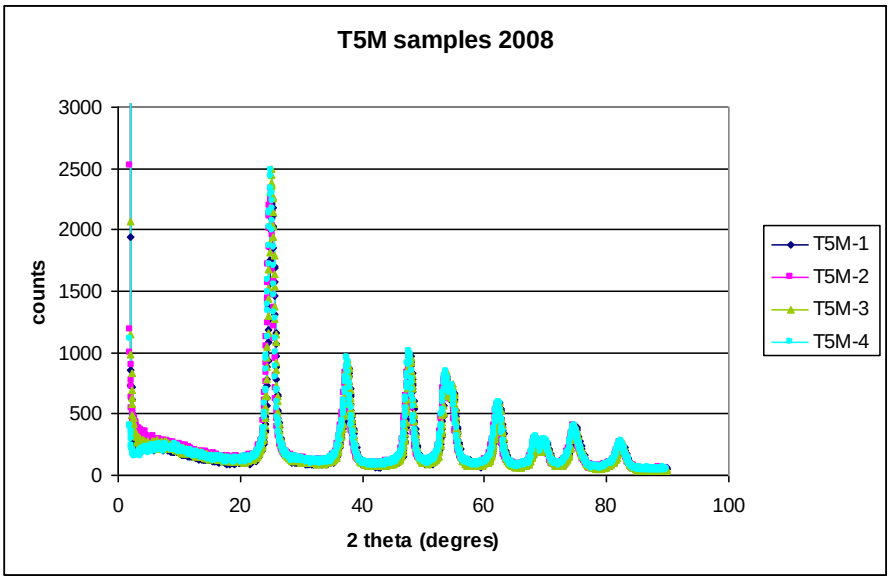

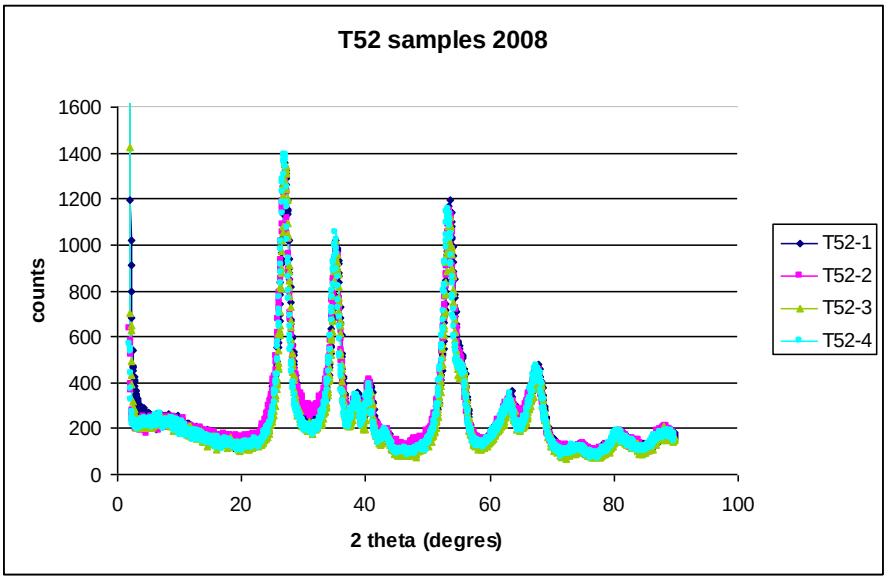

FIGURE 2 Measured XRD for T5M-Type (above) and T52-Type (below) Sorbent Materials from the Batches Received in 2008 [Note the relatively broad diffraction peaks (full width at half maximum of ~0.9° 2-theta). The diffraction patterns do not differ in any significant way from those on older batches reported on previously.]

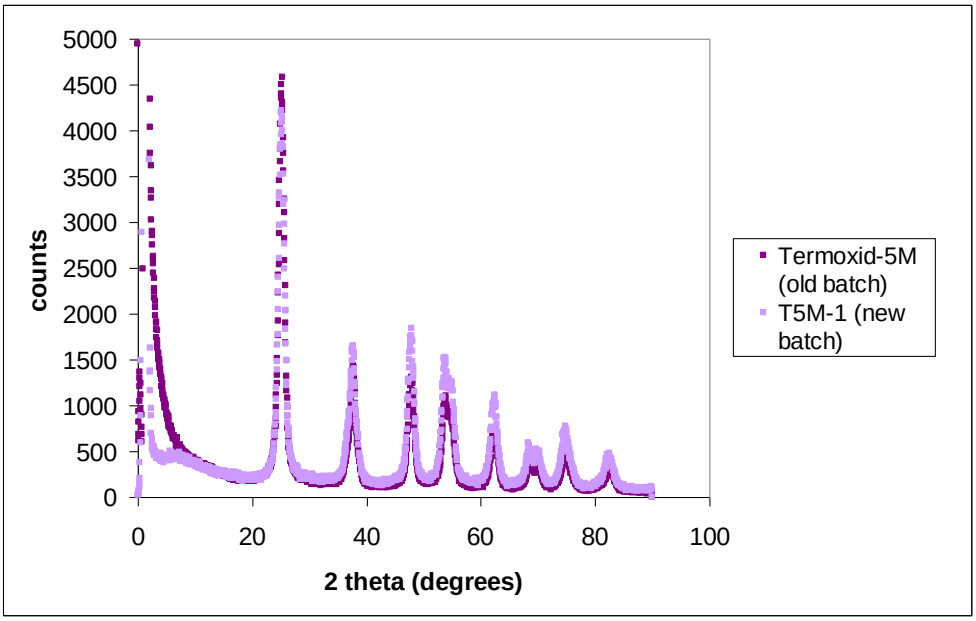

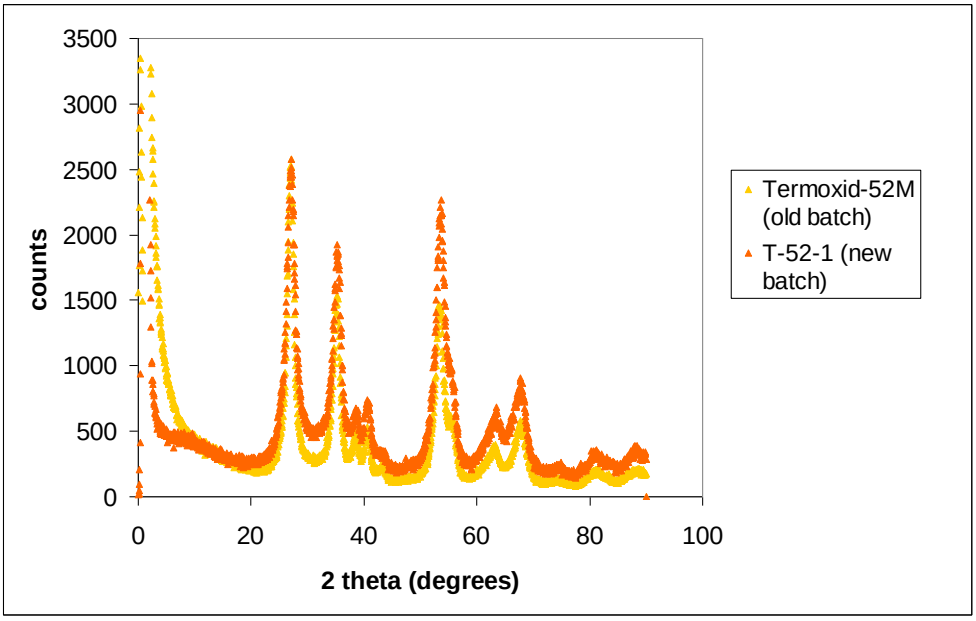

FIGURE 3 Measured XRD for T5M-Type (above) and T52-Type (below) Sorbent Materials Comparing Recent Batches with Representative Older Batches

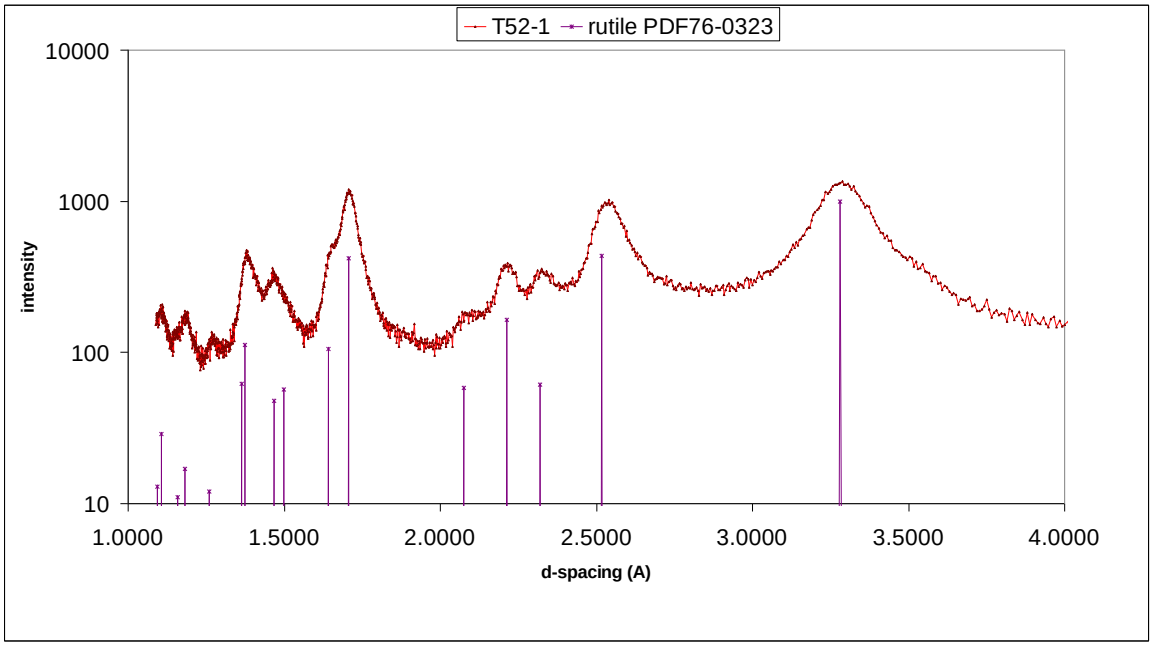

FIGURE 4 Comparison of T52 and Rutile

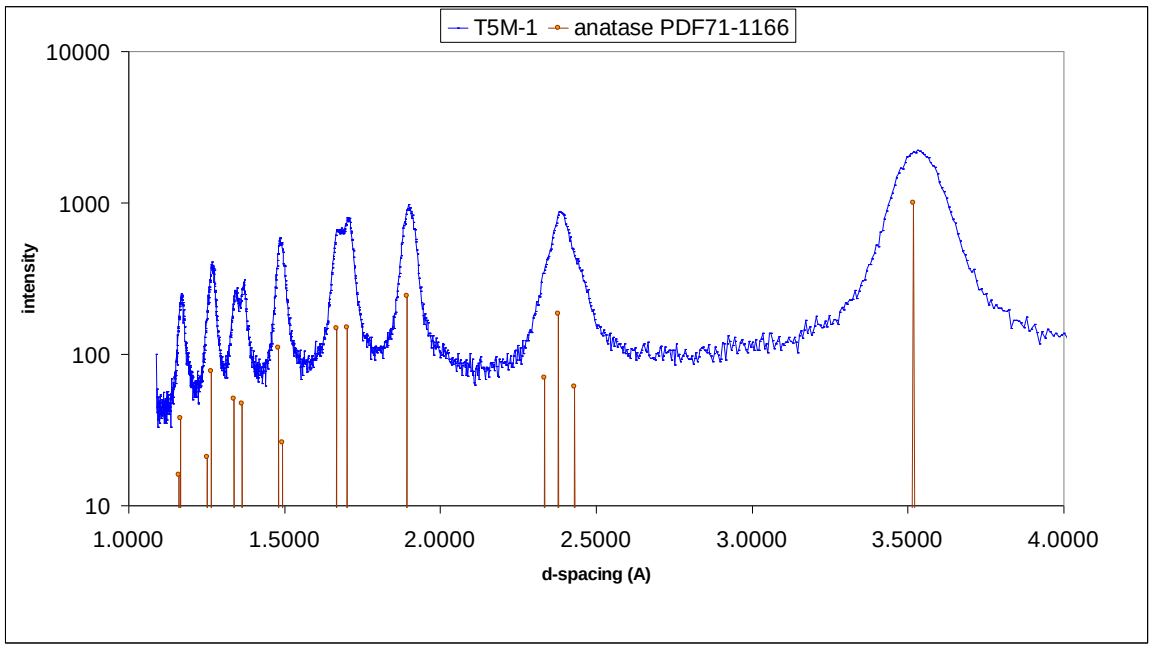

FIGURE 5 Comparison of T5M and Anatase

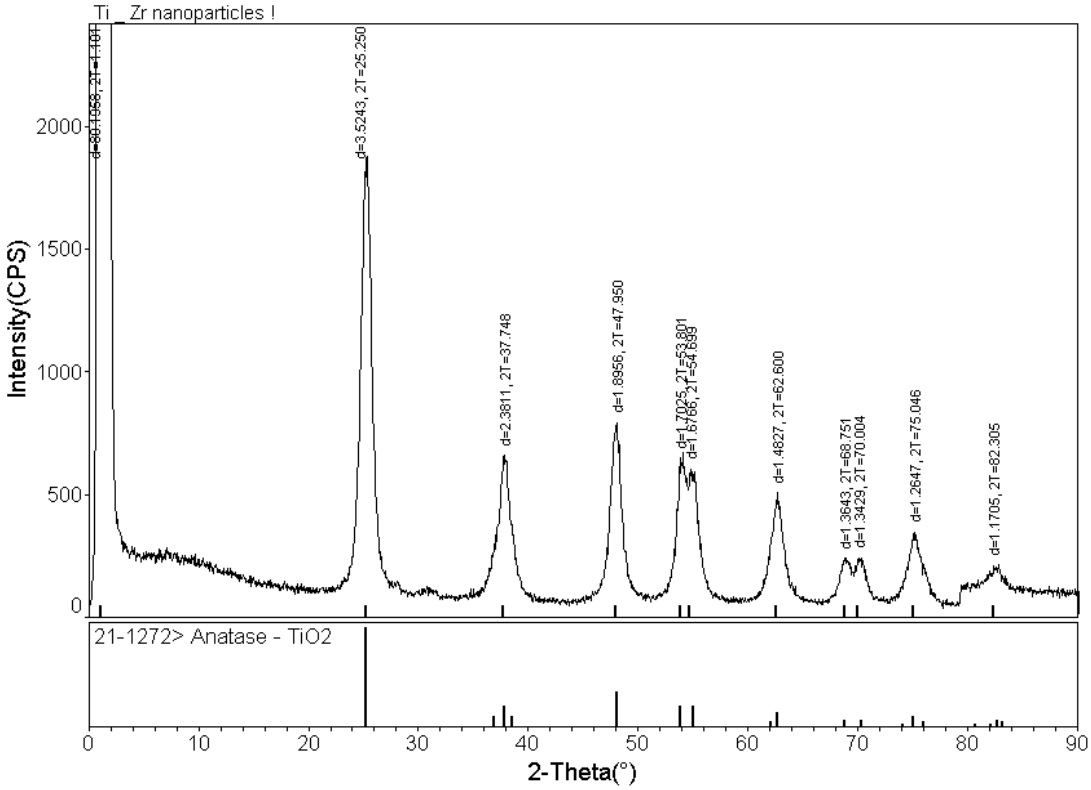

FIGURE 6 Comparison of S80 and Anatase

2.3 CONCLUSIONS

Both T5M and T52 sorbents by Termoxid are high-surface-area materials with a nanoscale substructure. As measured by XRD and BET, the physical properties of the batches provided did not display any intrinsic differences to which variations in the sorption efficacy of molybdenum could be attributed. XRD measurements indicate that T52 is a nanocrystalline version of rutile and that T5M and S80 are nanocrystalline versions of anatase.

3 UPTAKE OF Mo FROM URANYL NITRATE SOLUTIONS

Six sorbents are being evaluated to recover Mo(VI) from 60°C solutions containing 0.5 ppm Mo and 90 to 150 g-U/L at pH 1: (1 and 2) T-52 and T-5M (200–400 µm), (3 and 4) Adsorbsia (200 and 400 µm), (5) Sachtopore-80 (80 µm), and (6) alumina (75–150 µm). Results presented in Figure 7 indicate that T52, T5M, S80, and Adsorbsia sorbent can be used to design an efficient column. The K_d value of 272 for alumina from a 145 g/L U solution indicates that it would be difficult to design a separation system and that further work, including careful choosing of particle size, needs to be done.

3.1 EXPERIMENT

3.1.1 Preparation of Uranium Solutions

Uranyl nitrate or $UO_2(NO_3)_2$ solutions were prepared by dissolving a known amount of uranium metal plates in concentrated HNO_3. The solution was evaporated until it was dry, and the product was re-dissolved in distilled water (repeated three times). The resulting pH was about 0.9 and adjusted to pH 1 by using NaOH. $Na_2MoO_4 \cdot 2H_2O$ (Sigma-Aldrich) was added to the uranium solutions to obtain a 0.5-ppm Mo concentration.

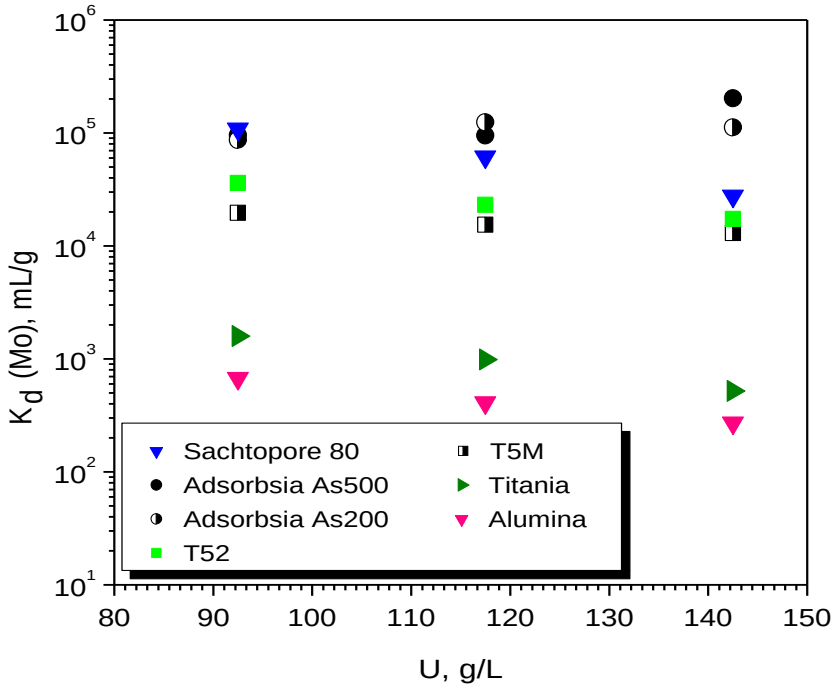

FIGURE 7 Uptake of 0.5 ppm Mo from a Uranyl Nitrate Solution at pH 1 and 60°C by Sorbents Being Considered for MIPS

3.1.2 Preparation of ^{99}Mo Spike Solution

^{99}Mo was obtained from a commercial ^{99m}Tc generator (Lantheus Medical Imaging, Inc.). The initial activity of Mo-99 in the generator was 1 Ci. ^{99}Mo was removed from the generator by placing a serum vial containing 1 M NH_4OH on the needle labeled "Saline Charge." Then an evacuated serum vial was placed on the needle labeled "Receiver." When no more bubbles appeared in the Saline Charge vial, the Receiver bottle was removed from the generator. The ^{99}Mo spiked solution was prepared by using a hot plate to make the obtained solution dry and then re-dissolving it in 0.1 M HNO_3.

3.1.3 Batch Uptake Measurements

The uptake of Mo(VI) as a function of uranium was determined by equilibrating 1 mL of a ^{99}Mo spiked aqueous solution with a known amount (10 ±1 mg) of sorbent for 24 hours at 55°C by using a thermostated shaker bath. The aqueous solutions contained 150, 195, 236, and 287 g-U/L and 0.5 ppm stable Mo. After equilibration, the solution was withdrawn and filtered by using a syringe fitted with a 0.22-µm pore size polyvinylidene fluoride (PVDF) membrane filter.

3.1.4 Counting of ^{99}Mo

The amount of activity in the aqueous samples was determined by using a germanium detector. ^{99}Mo was quantified by measurement of its 739 keV γ-ray. The activity of ^{99}Mo in each sample was corrected for decay. The extent of radionuclide uptake was expressed in terms of a distribution coefficient, K_d, defined as follows:

$$K_d = \left(\frac{A_o - A_s}{W}\right) \Big/ \frac{A_s}{V}$$

where Ao and As represent the aqueous phase activity (µCi) before and after equilibration, respectively, W is the dry weight of the sorbent (g), and V is the volume of the aqueous phase (mL).

4 LANGMUIR ISOTHERMS

Isotherm data in Table 2 were obtained by equilibrating 10 ± 1 mg of sorbent with 10 mL of solution containing 1.9 M $NaNO_3$, about 0.1 M HNO_3, and Na_2MoO_4 for 24 hours at 60°C. The Mo solutions in Table 2 were prepared by mixing a 0.1 M Mo solution with the nitrate solution. The pH of the solutions was varied as indicated in Table 2. The 0.1 M Mo solution was prepared by dissolving 0.1 mol Na_2MoO_4, 1.8 mol $NaNO_3$, and 1 L of 0.2 M HNO_3; the resulting pH was 1.3. The nitrate solution contained 1.9 M $NaNO_3$ and 0.1 M HNO_3. The pH of the nitrate solution was 0.81 due to high ionic strength.

Sorbents were also pre-equilibrated with the nitrate solution. In this experiment, a best attempt was made to keep the nitrate concentration constant, since it was initially thought that nitrate competes with Mo for sorption sites. This was not the best approach, because the nitrate concentration has very little effect on Mo adsorption. Through our recent experiments, we learned that even though HNO_3 does adsorb on titania (Vissenberg et al. 2000), the adsorption of Mo does not proceed via electrostatic interactions with the protonated groups. This fact is clearly illustrated by our nitrate dependency studies, which show that the sorption of Mo (at various concentrations) is independent of the nitrate concentration. Our data strongly suggest that Mo sorbs on titania sorbent through a reaction with the titania OH groups. Therefore, the most important factor in the adsorption of Mo is pH, which dramatically influences Mo speciation around a pH of 1. Nitrate still might have some effect on the sorption of Mo through the solubility of Mo at high ionic strength. In this experiment, the aqueous phase Mo concentration was obtained by counting ^{99}Mo tracer using a NaI gamma counter.

Isotherm data in Table 3 were obtained by equilibrating 10 ±1 mg of sorbent with 10 mL of solution containing 2 M $NaNO_3$, 0.09 M HNO_3, and Na_2MoO_4 at a pH of 1 for 24 hours at 60°C. Sorbents were pre-equilibrated with a solution containing 2 $NaNO_3$ and 0.09 M HNO_3. In this experiment, Mo concentrations were low and did not affect pH; therefore, the pH for all Mo solutions was 1. In this experiment, the aqueous phase Mo concentration was obtained by counting ^{99}Mo tracer using a NaI gamma counter.

Isotherm data in Table 4 were obtained by equilibrating 10 ±1 mg of sorbent with 1 mL of solution for 24 h at 60°C. The solution contained 1.3 M $NaNO_3$, 0.1 M HNO_3, and Na_2MoO_4. The pH of the solution was adjusted to 1 with NaOH solution. Sorbents were pre-equilibrated twice with 0.1 HNO_3 and 1.3 M $NaNO_3$. In this experiment, the aqueous phase Mo concentration was obtained by counting ^{99}Mo tracer using a NaI gamma counter.

Isotherm data in Table 5 were obtained by equilibrating 10 ±1 mg of sorbent with 1 mL of solution for 24 h at 60°C. The solution contained 1.3 M $NaNO_3$, 0.1 M HNO_3, and Na_2MoO_4. The pH of the solution was adjusted to 1 with NaOH solution. Sorbents were pre-equilibrated twice with 0.1 HNO_3 and 1.3 M $NaNO_3$. Aqueous Mo concentrations were measured by inductively coupled plasma–mass spectrometry (ICP-MS).

TABLE 2 Langmuir Isotherm Data Acquired by Equilibrating 10 mL of Solution Containing 1.9 M $NaNO_3$, 0.1 M HNO_3, and Na_2MoO_4 at Various pHs with Sorbent

		S80		T52		T5M	
[Mo], M	pH	Aqueous Equil Mo, M	Mols Mo/g sorbent	Aqueous Equil Mo, M	Mols Mo/g sorbent	Aqueous Equil Mo, M	Mols Mo/g sorbent
5.0E-05	0.81	1.0E-05	3.3E-05	8.9E-06	3.5E-05	8.9E-06	4.0E-05
1.0E-04	0.82	3.2E-05	6.2E-05	2.4E-05	7.7E-05	2.7E-05	7.4E-05
5.0E-04	0.83	2.3E-04	2.8E-04	2.0E-04	3.0E-04	1.6E-04	3.3E-04
1.0E-03	0.83	5.7E-04	3.8E-04	4.2E-04	5.8E-04	5.2E-04	5.0E-04
5.0E-03	0.83	4.1E-03	8.1E-04	4.0E-03	9.5E-04	3.8E-03	1.1E-03
1.0E-02	0.85	7.1E-03	2.7E-03	5.4E-03	4.3E-03	5.0E-03	4.8E-03
5.0E-02	1.0	3.0E-02	1.9E-02	1.9E-02	2.9E-02	3.1E-02	2.0E-02
1.0E-01	1.35	7.9E-02	2.0E-02	7.9E-02	2.1E-02	8.2E-02	1.7E-02

TABLE 3 Langmuir Isotherm Data Acquired by Equilibrating 10 mL of Solution Containing 2 M $NaNO_3$, 0.09 M HNO_3, and Na_2MoO_4 at a pH of 1 with Sorbent

		S80		T52		T5M	
[Mo], M	pH	Aqueous Equil Mo, M	Mols Mo/g sorbent	Aqueous Equil Mo, M	Mols Mo/g sorbent	Aqueous Equil Mo, M	Mols Mo/g sorbent
1.0E-05	1.0	1.6E-06	7.8E-06	6.4E-07	8.9E-06	6.8E-07	8.8E-06
1.0E-06	1.0	1.9E-07	7.5E-07	6.5E-08	9.4E-07	6.2E-08	9.2E-07
1.0E-07	1.0	1.7E-08	7.5E-08	7.3E-09	1.0E-07	4.2E-09	8.5E-08
1.0E-08	1.0	1.6E-09	9.6E-09	5.3E-10	8.5E-09	5.0E-10	9.8E-09
1.0E-09	1.0	9.3E-11	7.6E-10	8.1E-11	1.0E-09	6.0E-11	9.5E-10
1.0E-10	1.0	1.6E-11	9.6E-11	5.4E-12	9.4E-11	5.6E-12	9.3E-11

The data from Tables 2–5 are summarized in Figure 8. There seems to be a discrepancy between data obtained at 1.4 and 2 M NO_3^- in the 10^{-11} and 10^{-6} aqueous Mo concentration range. This difference is most likely due to the difference in volume/mass ratio between these two experiments. The experiment carried out at 2 M NO_3^- had a volume-to-mass ratio that was 10 times larger, which could result in less efficient mixing and lower sorption. Otherwise, slight variations in the pH of the solution could also account for differences in Mo uptake.

The increase in Mo uptake in the 10^{-3}–10^{-1} aqueous Mo concentration range is due to strong interactions between sorbed and aqueous Mo species, resulting in the formation of a crystalline layer on the sorbent surface, as shown in the scanning electron microscope (SEM) image in Figure 9.

TABLE 4 Langmuir Isotherm Data Acquired by Equilibrating 1 mL of Solution Containing 1.3 M $NaNO_3$, 0.1 M HNO_3, and Na_2MoO_4 at a pH of 1 with Sorbent

	S80		T52		T5M		As500		As200		AG4	
[Mo], M	Aqueous Equil Mo, M	Mols Mo/g sorbent	Aqueous Equil Mo, M	Mols Mo/g sorbent	Aqueous Equil Mo, M	Mols Mo/g sorbent	Aqueous Equil Mo, M	Mols Mo/g sorbent	Aqueous Equil Mo, M	Mols Mo/g sorbent	Aqueous Equil Mo, M	Mols Mo/g sorbent
1.0E-03	2.0E-06	1.0E-04	2.5E-06	9.0E-05	7.6E-06	1.1E-04	1.3E-06	1.1E-04	4.5E-07	9.8E-05	1.1E-04	8.4E-05
1.0E-04	6.1E-08	1.2E-05	1.0E-07	9.6E-06	2.3E-07	1.0E-05	6.9E-08	1.1E-05	5.1E-08	1.0E-05	4.4E-07	8.2E-06
1.0E-05	1.4E-08	1.1E-06	6.4E-09	1.0E-06	8.9E-09	9.0E-07	4.5E-09	1.1E-06	9.6E-09	9.8E-07	1.4E-08	9.2E-07
1.0E-06	6.4E-10	9.8E-08	8.8E-10	1.1E-07	1.0E-09	1.0E-07	4.9E-10	1.0E-07	7.1E-10	1.1E-07	9.6E-10	9.3E-08
1.0E-07	7.2E-11	1.1E-08	1.7E-10	1.1E-08	1.9E-10	1.0E-08	6.6E-11	1.0E-08	5.8E-11	1.1E-08	6.0E-11	8.1E-09
1.0E-08	7.8E-12	9.4E-10	1.8E-11	1.0E-09	1.8E-11	1.0E-09	1.3E-11	1.0E-09	1.4E-11	1.2E-09	8.1E-12	8.9E-10
1.0E-09	7.4E-13	1.1E-10	9.2E-13	1.0E-10	5.4E-12	1.1E-10	1.3E-12	1.2E-10	1.5E-12	1.1E-10	8.3E-13	9.1E-11
1.0E-10	1.1E-13	9.7E-12	1.5E-13	9.2E-12	1.3E-13	1.2E-11	9.1E-14	9.3E-12	1.5E-13	9.9E-12	6.6E-14	8.1E-12

TABLE 5 Langmuir Isotherm Data Acquired by Equilibrating 1 mL of Solution Containing 1.3 M $NaNO_3$, 0.1 M HNO_3, and Na_2MoO_4 at a pH of 1 with Sorbent

		S80		T52		T5M		AG4	
[Mo], M	pH	Aqueous Equil Mo, M	Mols Mo/g Sorbent	Aqueous Equil Mo, M	Mols Mo/g Sorbent	Aqueous Equil Mo, M	Mols Mo/g Sorbent	Aqueous Equil Mo, M	Mols Mo/g Sorbent
0.00194	1.0	2.5E-05	2.1E-04	1.7E-05	2.0E-04	1.7E-05	2.1E-04	5.5E-04	1.5E-04
0.00384	1.0	1.8E-04	3.9E-04	8.0E-05	3.3E-04	8.4E-05	3.8E-04	6.8E-04	3.0E-04
0.00553	1.0	3.1E-04	5.1E-04	3.5E-04	5.4E-04	3.1E-04	5.8E-04	7.4E-04	3.9E-04
0.00699	1.0	5.2E-04	6.1E-04	8.0E-04	6.1E-04	7.6E-04	6.6E-04	9.6E-04	5.8E-04
0.00879	1.0	1.1E-03	8.0E-04	8.9E-04	7.1E-04	7.9E-04	8.7E-04	1.1E-03	7.7E-04
0.01010	1.0	1.3E-03	8.3E-04	9.5E-04	8.7E-04	8.1E-04	9.3E-04	1.2E-03	7.7E-04

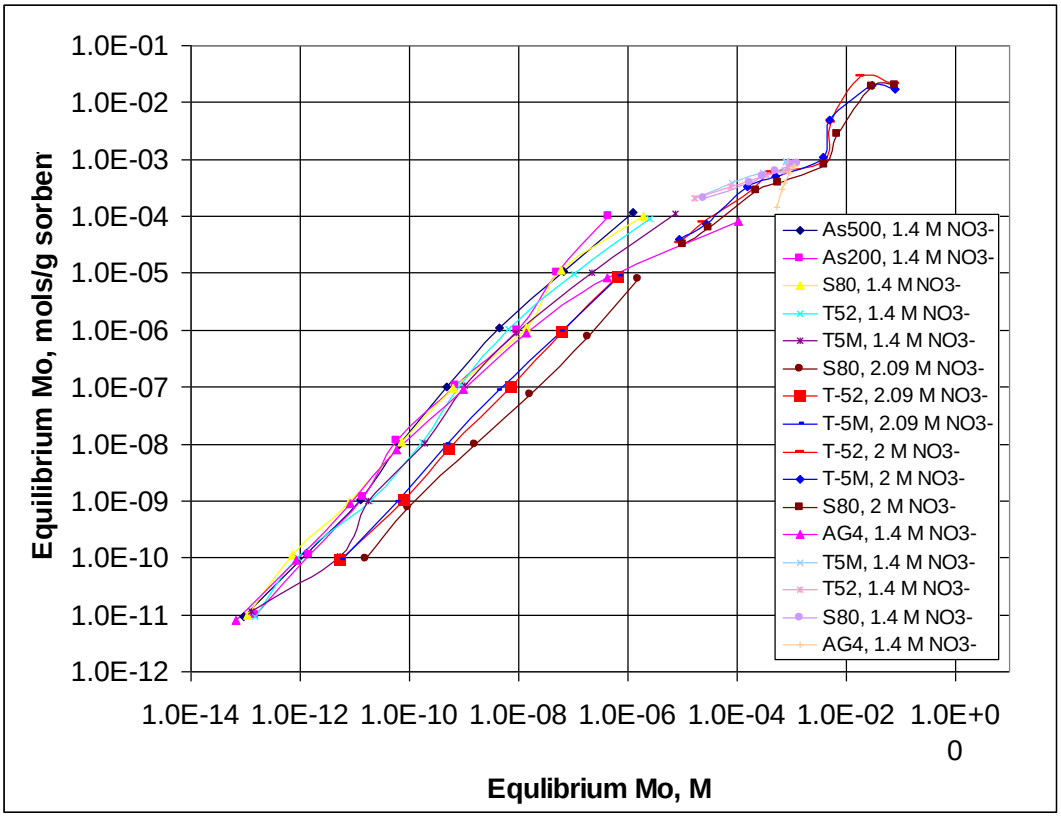

FIGURE 8 Combined Results of Langmuir Isotherm Data

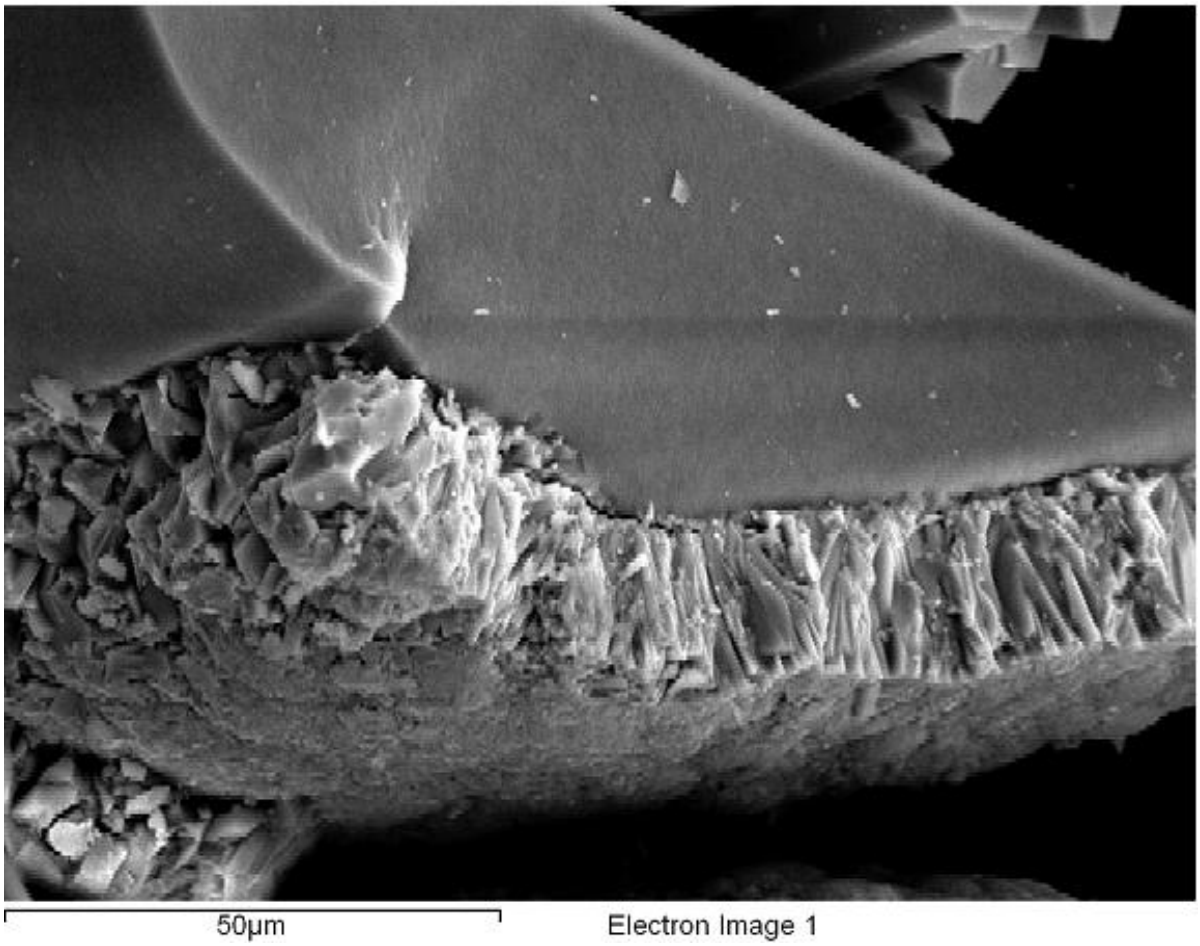

FIGURE 9 Scanning Electron Microscope Image of Mo Precipitated Layer on the Surface of T5M Sorbent

5 CHEMICAL STABILITY

5.1 SORBENT STABILITY TO pH 1 AND 14 WASHING CYCLES

The chemical stability of T5M, T52, and S80 was determined by exposing the sorbents to cycles of contacts with 0.1 M HNO_3 (stirring for 3 h at 60°C) and 1 M NaOH (stirring for 1 h at 60°C), as shown in Figure 10. Sorbents were exposed to 0, 3, 5, and 10 cycles of washes. Their K_d values were determined by contacting the sorbents with 1 ppm Mo in 0.1 M HNO_3 solution for 24 h at 60°C. After three cycles, a significant drop in K_d values occurred. However, the K_d values did not decrease further upon exposure to HNO_3 and NaOH, indicating that the sorbents were stable under the conditions investigated here.

Adsorbsia sorbents were also evaluated for their chemical stability during this experiment. However, after the first cycle of 0.1 M HNO_3 and 1 M NaOH washing, these sorbents degraded and formed a fine powder.

The initial drop in K_d values was most likely due to the fact that the titania sorbents without pretreatment were also not pre-equilibrated with HNO_3. The unequilibrated sorbents adsorbed HNO_3, which caused an increase in both the pH of the Mo solution and the concentration of the sorbing Mo species. Alternatively, the drop in K_d values could be due to oxidative restructuring of reduced titania sites by nitric acid. The structure of TiO_2 is quite complex and contains various types of defects, such as oxygen vacancies and TiO_{2-x}, Ti^{3+}, and Ti^{4+} interstitials (Diebold 2003). The coordinatively unsaturated sites (CUSs) and Ti^{3+} participated in the sorption of Mo (Vissenberg et al. 2000). The loss of the CUSs by oxidation with nitric acid can result in lower K_d values.

5.2 DISCOLORATION OF Mo SOLUTION

Several observations were made during the "sorbent stability to pH 1 and 14 washing cycles." When T52 and T5M, previously exposed to 5 and 10 washing cycles, came in contact with 1 ppm Mo in 0.1 M HNO_3 for 24 h at 60°C, the Mo solutions became yellow. Similarly, when S80 was exposed to 10 cycles of washing and came in contact with 1 ppm Mo in 0.1 M HNO_3 for 24 h at 60°C, the sorbent appeared yellow/orange.

Solutions from K_d measurement were submitted for ICP-MS analysis. The results (Table 6) indicate that the composition of the aqueous phase was similar to that observed previously when the sorbents were exposed to 0.1 M HNO_3, in the absence of Mo, for several days at room temperature. These results suggest that sorbent leaching into the aqueous phase was not responsible for the color change.

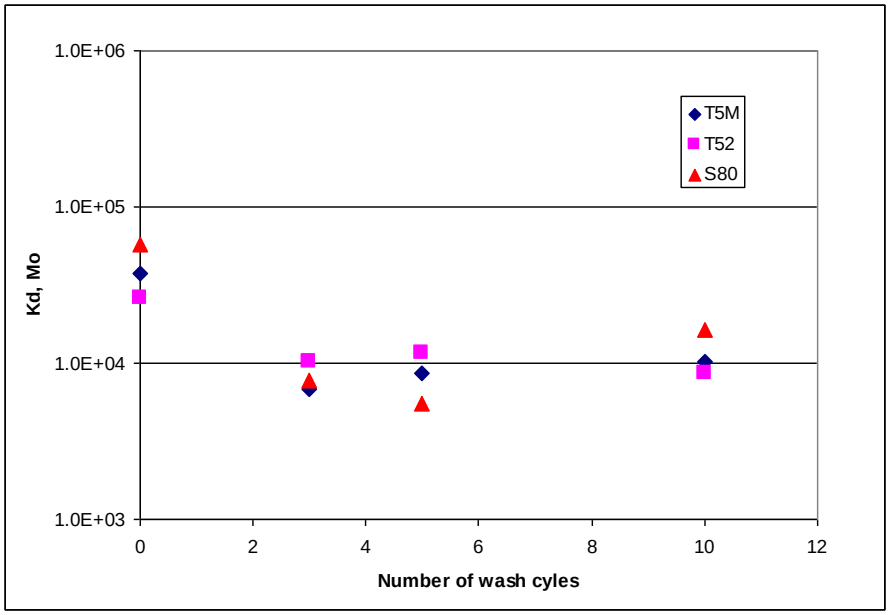

FIGURE 10 Sorbent Stability after Exposure to pH 1 and pH 14 Washing Cycles

TABLE 6 Composition of 0.1 M HNO_3 and Mo Solutions after Contact with Sorbents

Sample ID	Ti (ppb)	Zr (ppb)	Sn (ppb)
T5M*	363	8.02	<0.68
T5M-5	345	28.9	<0.68
T5M-10	307	32.2	<0.68
T52*	185	8.51	1
T52-5	211	9.72	0.81
T52-10	222	8.02	<0.68
TiO_2 sorbent[a]	268	7.29	<0.68
TiO_2 sorbent-10	176	9.44	<0.68

[a] Contacted with 0.1 M HNO_3, several days at room temperature Sorbent-5 and Sorbent-10 indicates number of cycles washing with 0.1 M HNO3 (3h, 60°C) and 1 M NaOH (1h, 60°C).

The change in color identified during the K_d experiments had also been randomly observed during previous experiments. It was noted that the color change occurred only in the presence of Mo. Therefore, several experiments were set up to elucidate the trend of the color change in the Mo solutions. The following observations were made:

1. When contacted with T52, T5M, and S80 at 25°C and 60°C for 24 h, 2 M sodium nitrate solution at pH 1 does not change color.

2. In the absence of sorbent, 0.01 Mo solution containing 2 M sodium nitrate at pH 1 changes color (yellow) and forms a precipitate after several weeks/months.

3. When contacted with sorbent at 60°C, 0.01 Mo solution containing 2 M sodium nitrate at pH 1 changes color (yellow) and forms a precipitate within 24 h.

4. When contacted with sorbent at room temperature, 0.01 Mo solution containing 2 M sodium nitrate at pH 1 changes color (yellow) and forms a precipitate within days/weeks.

5. The color of the Mo solution changes more readily in the presence of a sorbent and the presence of increased concentrations of sodium nitrate and/or sodium molybdate.

These results indicate that changes in solution color occur only in the presence of Mo. Therefore, the properties of Mo in solution at pH 1 are affected by the presence of the sorbents, and the changes are accelerated by high ionic strength and increased temperature.

These results described above indicate that the color change observed was a result of a modification in the structure of H_2MoO_4. This change was most likely caused by a loss of water of hydration and the formation of a yellow $MoO_3 \cdot n\text{-}xH_2O$ species from a white $MoO_3 \cdot nH_2O$ solution species. Various $MoO_3 \cdot nH_2O$ complexes have been described in the literature with their structures, water of hydration numbers, crystal structures, and subsequently colors, which vary depending on the preparation conditions (Yebka et al. 1999; Weast et al. 1964). Under MIPS conditions, these changes are accelerated by high nitrate and Mo concentrations through the lowered activity of water and the presence of sorbent. These structural variations of H_2MoO_4 do not have negative effects on Mo sorption and are not expected to interfere with Mo recovery.

The possibility that Mo(VI) is reduced to Mo(V) under the conditions described above was ruled out by adding 1 M SCN^- to a Mo solution that had been in contact with sorbents. Complex formation between Mo(V) and thiocyanate is described by Equation (1) (Hiskey and Meloche 1940). No change in color upon the addition of thiocyanate to the Mo solution was observed. Furthermore, the same Mo solution was treated with ascorbic acid, followed by addition of 1 M SCN^- solution. Under these conditions, the color of the solution turned to green/blue, indicating the presence of reduced Mo species.

$$[Mo^{5+}R]^{n+} + n(SCN^{-}) \leftrightarrow [Mo^{5+}R](SCN)_n + x(OH^{-}) \quad (1)$$

5.3 SOLUBILITY OF TiO_2

The speciation diagrams (solid is in excess) shown in Figures 11 and 12 were made by using relatively new stability constants for titanium aqueous species at 25°C. Based on Figures 11 and 12, it is possible to get measurable dissolved concentrations of titanium by leaching it with a 0.1 M nitric acid solution. As indicated by the solubility diagrams and data reported by Sugimoto et al. (2002), the solubility of hydrous TiO_2 is nearly proportional to the second power of the acid concentration below pH 2. Therefore, treatment of titania with acid solutions below pH 1 is not recommended.

The solubility diagrams of rutile and anatase are consistent with the composition of the aqueous phase after contact with T5M (anatase) and T52 (rutile) determined by ICP-MS in Table 6. The results show that levels of Ti in solution are about 50% higher for T5M (anatase) than T52 (rutile) and indicate that T52 is more stable than T5M is.

The ICP-MS results do, however, suggest that S80 (anatase) is as stable as T52 (rutile). This finding could be due to more uniform particles and less loose nanoparticles with a high surface area.

These results can be also reinforced by the Mo K_d experiments for T52 and T5M from uranyl nitrate solutions (150, 185, 235, and 285 g-U/L at pH 1) at 25°C, 55°C, and 85°C (Figure 13). From 25°C to 55°C, K_d values for T52 increase. However, for T5M at 85°C, the Mo K_d values decrease, suggesting greater sorbent degradation for T5M (anatase) than for T52 (rutile).

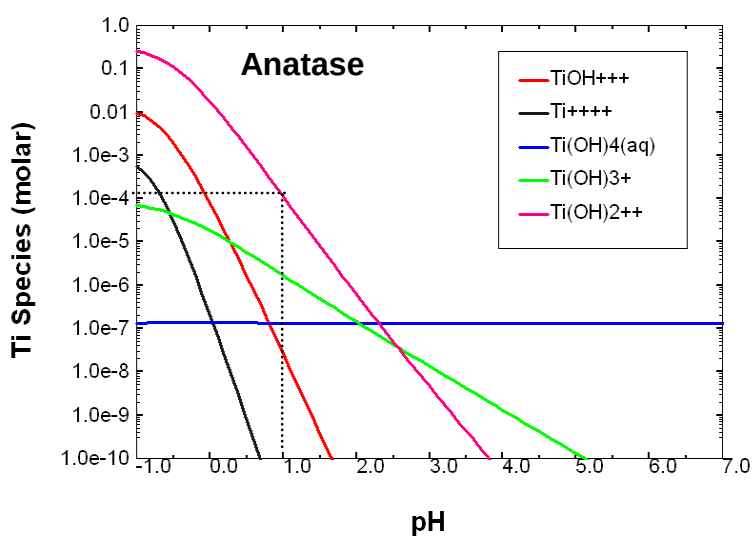

FIGURE 11 Speciation Diagram for Titania Anatase Modification at 25°C

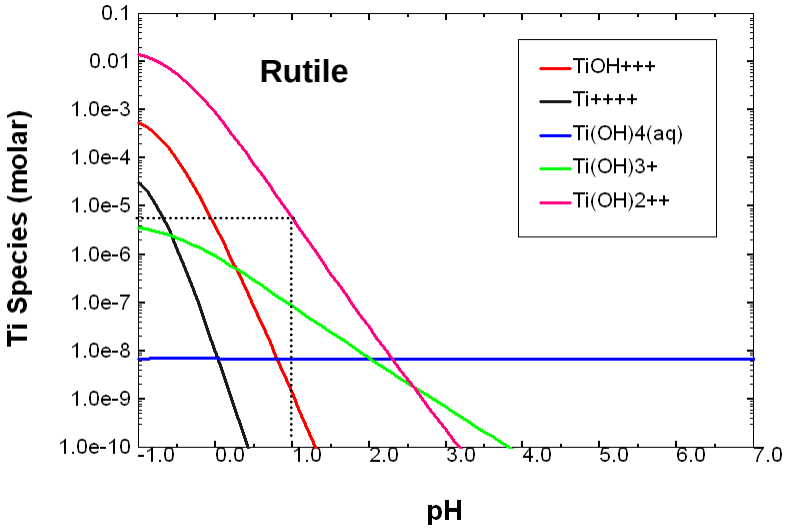

FIGURE 12 Speciation Diagram for TitaniaRutile Modification at 25°C

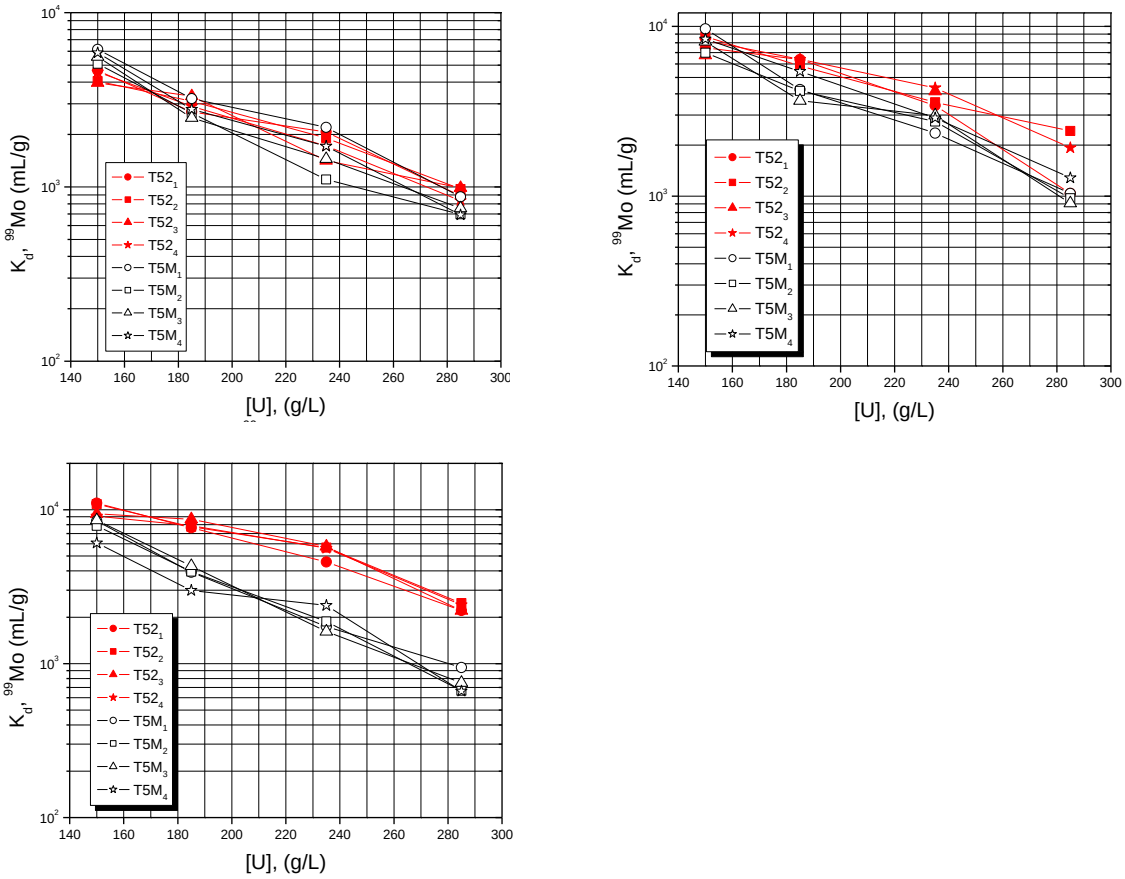

FIGURE 13 Uptake of Mo as a Function of Uranyl Nitrate Concentration at pH 1 and 25°C, 55°C, and 85°C (clockwise) for Batches of T52 and T5M ($T52_1$–$T52_4$ and $T5M_1$–$T5M_4$)

5.4 EXPERIMENTS OF SORBENT LEACHING DURING UPTAKE OF COMPETING COMPONENTS

Sorbents were also exposed to a simulated fuel solution at 60°C, 24 h, and pH 1 and were analyzed by ICP-MS for Ti, Zr, and Sn. The solution that came in contact with T52 contained 470 μg/L Ti and 202 μg/L Sn, the one that came in contact with T5M contained 816 μg/L Ti and 49 μg/L Zr, and the one that came in contact with S80 contained 429 μg/L Ti. These results agree with the data presented throughout this section and confirm that T52 and S80 are chemically more stable than is T5M.

5.5 DECREASE OF COLUMN VOID FRACTIONS

A decrease in column void fractions was observed on Column 1 (T5M sorbent) after 8 weeks of testing in the presence of 0.01 HNO_3, 0.01 M HCl, or 0.01 M NaOH. The total column void fraction, ε_t, total column void fraction, was reduced from 0.76 to 0.72 (uracil pulses) or 0.68 ($NaNO_3$ pulses), whereas the interparticle void fraction, ε_b, was slightly reduced from 0.30 to 0.28. Possible causes of the decrease in column void fractions were that the HCl pretreatment might be harmful for the sorbent and that the sorbent cannot tolerate frontals of 0.01 N HNO_3 (pH 2) and 0.01 N NaOH stripping (pH 12). After prolonged use of T52, a decrease in the column void fraction was not observed for T52.

6 RADIOLYTIC STABILITY

The radiolytic stabilities of T5M, T52, S80, and AG4 were determined by contacting the sorbents, ~10 mg, with 150 g-U/L uranyl nitrate solution and irradiating them at the Van de Graff. The irradiation doses were 311 kGy and 1.15 MGy. After irradiation, the uranium solution was removed and a new solution containing 150 g-U/L, 0.7 ppm Mo and Mo-99 at pH 1 was added to the sorbents. The sorbents were equilibrated for 24 h at 60°C, and K_d values were obtained as described in Section 3 (Uptake of Mo from Uranyl Nitrate Solutions). The results in Figure 14 indicate that within the irradiation doses investigated, the sorbents do not lose their Mo sorption properties, as shown by the constant (within experimental error) K_d values.

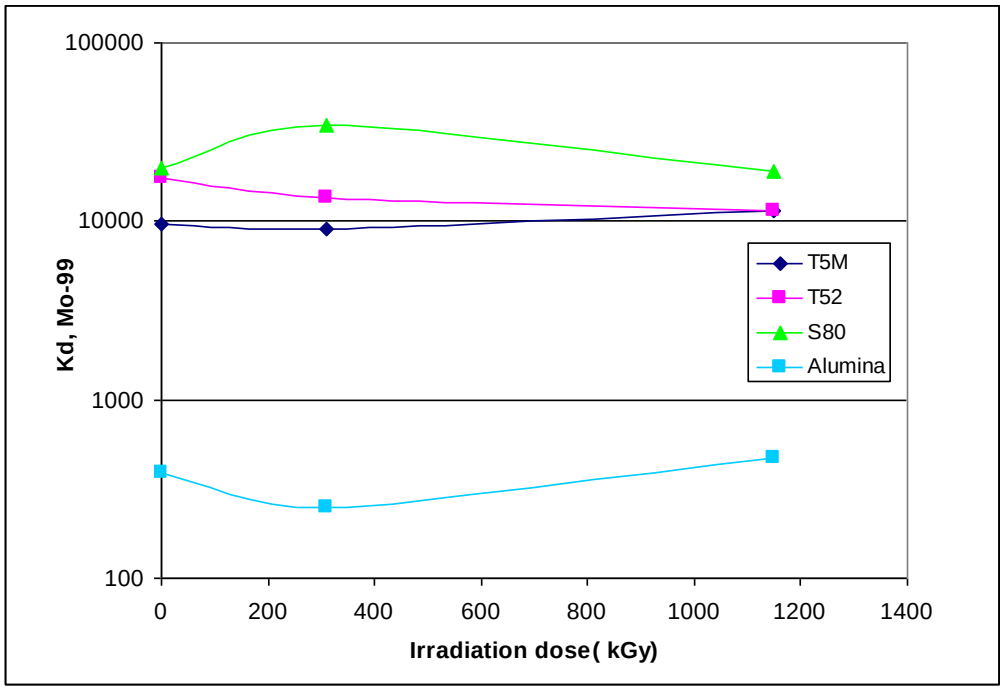

FIGURE 14 Effect of Radiation Dose on Uptake of Mo

7 URANIUM RECOVERY

7.1 BATCH STUDIES

The uptake of uranium was determined as a function of HNO_3 concentration. The results in Figure 15 and Table 7 indicate that uranyl nitrate sorbs on T5M and S80 sorbents. At 0.01 M HNO_3, S80 and T5M had U-233 K_d values of 365 and 107, respectively, whereas T52 and AG4 displayed K_d values of about 10. U adsorption from 0.1 M HNO_3 also shows a significant variation between T5M and S80 versus T52 and AG4, with T5M and S80 exhibiting about 20 times higher uptake. At 1 M HNO_3, uranium K_d values were about the same for all sorbents evaluated here. These results indicate that uranium can be efficiently washed from T52 and AG4 by using 0.1 M HNO_3. S80 and T5M should be washed with 1 M HNO_3 in order to efficiently remove uranyl nitrate from the column.

7.2 COLUMN STUDIES

The results of batch studies on the uptake of uranyl nitrate by the sorbents were confirmed by small column experiments, as shown in Figure 16. As expected, uranyl nitrate was eluted faster from a T52 loaded column than from a T5M column. Unexpectedly, a uranyl nitrate peak emerged earlier from a T5M column than from an AG4 column, even though T5M had K_d values that were one order of magnitude higher than those obtained for AG4. This can be explained by channeling of uranium through the larger sorbent particles of T5M (0.2–0.4 mm). In fact, the long uranium tail on a T5M packed column and the higher amount of HNO_3 needed to elute uranium from T5M as compared to AG4 confirmed the results of batch studies. High K_d values for S80 sorbents were also confirmed by the column tests. The elution of uranyl nitrate from S80 was not complete after 10 bed volumes of 0.1 M HNO_3, and only 76 ± 5% of uranium was recovered. The elution was completed by passing an additional 10 bed volumes of 1 M HNO_3.

Uranium was also completely recovered from T5M, T52, and AG4 sorbents (Table 8). The need to use 1 M HNO_3 to remove uranium from a S80 column does not automatically disqualify its use in the MIPS, since the recovered uranyl nitrate in 1 M HNO_3 solution can be used to adjust the pH of reactor fuel solution. However, the solubility of S80 under those conditions might be a concern, as discussed in Section 5 (Chemical Stability), and it will be investigated further.

In addition, scrubbing S80 with 1 M HNO_3 leads to a loss of Mo. When S80 loaded with Mo to about 5×10^{-7} mol Mo/g sorbent (conditions relevant to MIPS) comes in contact with 1 M HNO_3 (24 h, 60°C), 1.5% of the Mo is desorbed.

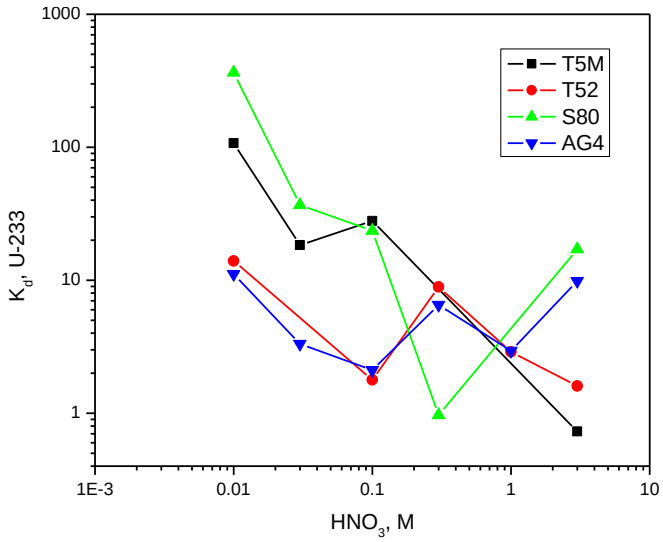

FIGURE 15 Uptake of Tracer Levels of U-233 (60°C, 24 h) from HNO_3 Solutions

TABLE 7 Uptake of Tracer Levels of U-233 (60°C, 24 h) from HNO_3 Solutions

	Kd Values			
HNO_3, M	T5M	T52	S80	AG4
0.01	107	14	365	11
0.03	18	0	37	3
0.1	28	2	24	2
0.3	0	9	1	7
1	0	3	0	3
3	1	2	17	10

7.3 EXPERIMENT

Recovery of uranyl nitrate was determined by loading 50 µL of a 150 g-U/L solution spiked with U-233 onto a column filled with 2 ml bed volume of sorbent. Sorbents were loaded into the columns as slurry in 0.1 M HNO_3. Uranyl nitrate was eluted off the column by using 0.1 M HNO_3. Uranyl nitrate from S80 was eluted with an additional 10 bed volumes of 1 M HNO_3. ^{233}U was quantified by measuring its α emission on a Perkin-Elmer liquid scintillation counter.

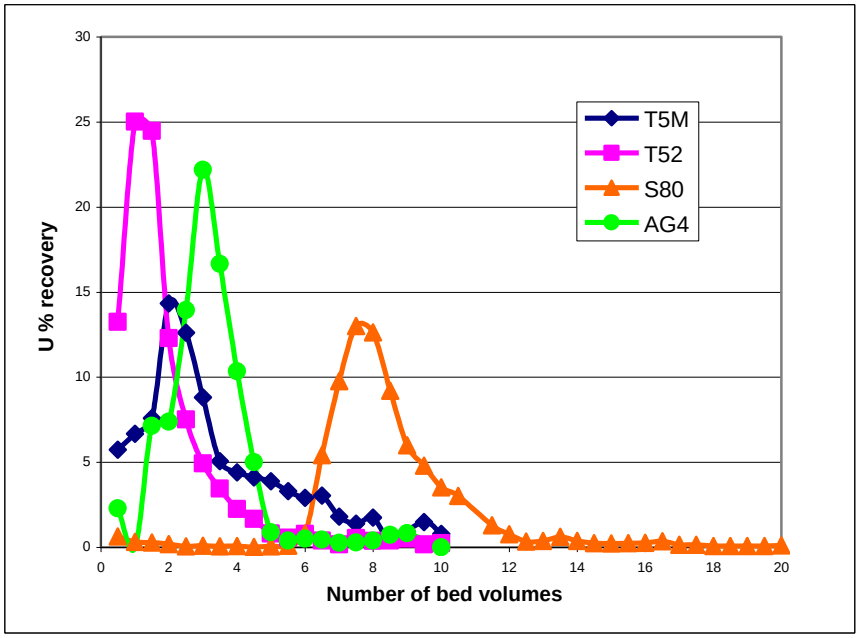

FIGURE 16 Elution of Uranium from T5M, T52, S80, and AG4

TABLE 8 Recovery of Uranyl Nitrate from T5M, T52, S80, and AG4

No. of Bed Volumes	T5M (% recovery)	T52 (% recovery)	S80 (% recovery)	AG4 (% recovery)
10	97 ± 5	100 ± 5	76 ± 5	96 ± 5
20			93 ± 5	

8 X-RAY DIFFRACTION ANALYSIS OF SORBENT RESIDUE

Fines from the T52 sorbent were filtered out of the uranyl nitrate solution used in column tests. The material was a fine white powder and mildly radioactive. There was just enough material to cover a glass x-ray diffraction slide, which was then covered with a polypropylene film to prevent the spread of radioactive contamination into the x-ray diffractometer. Radiation protection protocol required that the sample preparation be done in a fume hood, which was far from optimal for handling fine powder and static-cling film. Remaining fines in the bottle were rinsed with deionized water and transferred to a clean bottle for later examination using electron microscopy. The glass slide with powder was submitted to the Argonne Analytical Chemistry Laboratory for x-ray diffraction analysis.

The resulting diffraction pattern consisted of weak, sharp peaks arrayed upon a strong background arising from the sample holder/polypropylene film. The pattern is shown in Figures 17 and 18, along with the peak positions for two common mineral forms of TiO_2 (anatase and rutile). Also shown in the figures are the diffraction patterns from the T52 and the T5M sorbents, which consist of extremely broad peaks arising from the nanocrystalline structure of the material (Vandergrift et al. 2008).

Several striking observations can be made from the data:

- The material appears to consist mainly of a mixture of anatase and rutile, which is a rather unexpected result since anatase is more commonly observed to precipitate at low temperatures, while rutile is considered a high-temperature phase.

- The T52 type sorbent appears to be based on a nanocrystalline form of rutile.

- The T5M type sorbent appears to be based on a nanocrystalline form of anatase.

If the T52 sorbent was indeed the parent material, it is possible that the residue was formed by the decomposition of the nanocrystalline structure. This would explain how rutile formed at a low temperature. The appearance of anatase was likely due to the concurrent dissolution and re-precipitation of the form closer to thermodynamic equilibrium. If this is true, then the T5M sorbent should not produce a precipitate—or an anatase-only residue under similar conditions—owing to the absence of a rutile framework on which to build.

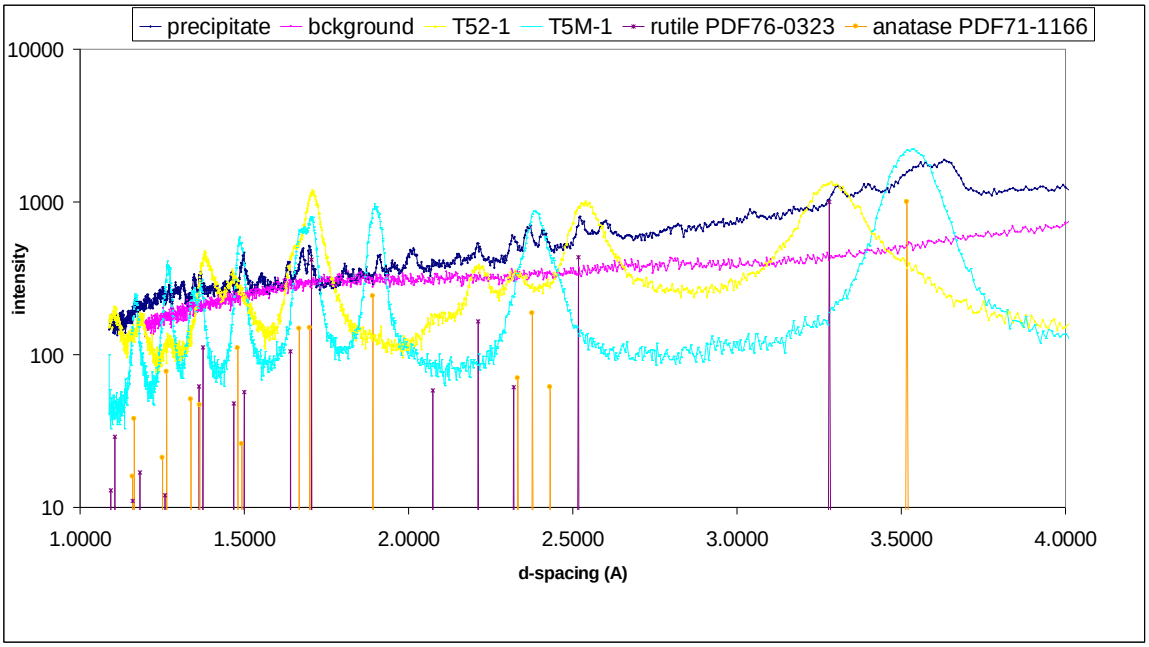

FIGURE 17 Comparison of X-ray Diffraction from the Precipitate (dark blue) with That Obtained from a Blank Sample Holder (magenta) and the T5M (light blue) and T52 (yellow) Sorbents [Also shown are the diffraction peak positions for two different crystal forms of TiO_2 rutile (dark purple) and anatase (orange), according to the JCPDS-ICDD reference database.]

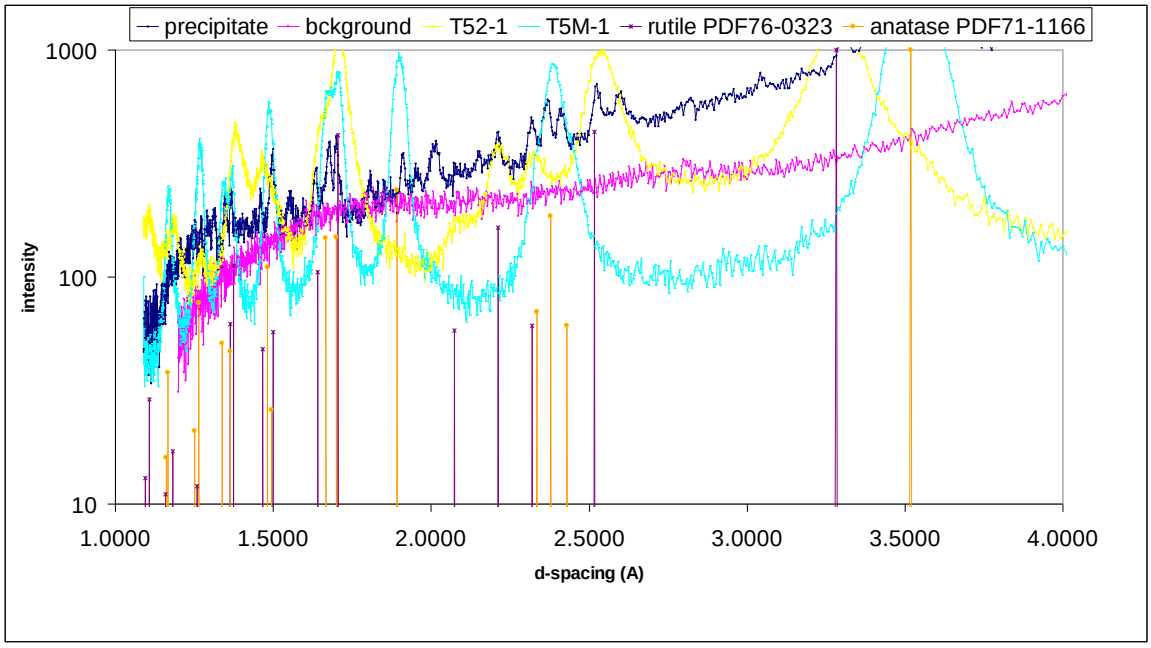

FIGURE 18 X-ray Diffraction Detail (Same key as that in Figure 16)

9 DYNAMIC LIGHT SCATTERING ANALYSIS OF T52 AND T5M AQUEOUS SUSPENTIONS

9.1 INTRODUCTION

Aqueous solutions vigorously shaken with T52 and T5M appear cloudy, whereas gently swirled samples appear clear. This indicates that sorbent nanoparticles are present in the samples and that their amounts are related to the physical treatment and mechanical stability of the sorbent. Also, the suspension of T52 appears clear after filtering with a 1-μm filter. Consistent with these observations are results from dynamic light scattering (DLS) measurements (Table 9). A first wash of T52 contains large nanoparticles that are about 2,000 nm in size, and a second wash still produces nanoparticles in the 40- to 300-nm range (Figures 19–24). The T5M suspension remains cloudy after filtering with a 1-μm filter but is clear after filtering with a 0.2-μm filter. This is also consistent with DLS results shown in Figures 25–30: After the first wash, particles are in the 200- to 800- nm range, and in the second wash, particles range from 100 to 1000 nm.

9.2 CONCLUSIONS

Titania nanoparticles might be present in the reactor solution as a result of (1) the mechanical degradation of the sorbent or (2) the reactor solution becoming supersaturated with respect to titanium hydroxide, which can form a precipitate (as observed during column studies). The effects of titania (or alumina) nanoparticles in the reactor solution from mechanical sorbent degradation or precipitation are not understood. The methods used to remove nanoparticles and/or prevent their formation and subsequent precipitation in the reactor solution will depend on the levels that can be tolerated in the reactor solution.

TABLE 9 Summary of Dynamic Light Scattering Results for T52 and T5M Samples

Sample ID	Wash No.	Diameter (nm)	Polydispersity	Fit
T52	1	~2000	0.29	Poor
T52	2	184	0.26	Monomodal
		50 (14%)	0.26	Multi-size distribution
		258 (86%)		
T5M	1	419	0.22	Monomodal
		250 (44%)	0.22	Multi-size distribution
		773 (56%)		
T5M	2	258	0.18	Monomodal

Sample ID	T-52M_1st wash_diluted #1A (Combined)
Operator ID	mertz
Elapsed Time	00:10:00
Median Diam.	1905.8 nm
Mean Diam.	2166.3 nm
Polydispersity	0.292
GSD	1.659

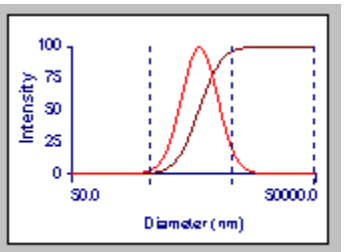

d(nm)	G(d)	C(d)	d(nm)	G(d)	C(d)	d(nm)	G(d)	C(d)
828.8	26	5	1676.7	97	40	2680.7	80	75
995.9	44	10	1788.0	99	45	2918.6	70	80
1128.0	58	15	1905.8	100	50	3219.8	58	85
1244.4	70	20	2031.3	99	55	3646.8	44	90
1354.9	80	25	2166.2	97	60	4382.4	26	95
1461.8	87	30	2315.9	93	65			
1568.3	93	35	2484.7	87	70			

Intensity

Copy for Spreadsheet

FIGURE 19 Monomodal Size Distribution for T52, First Wash

T-52M_1st wash_diluted #1A (Combined)

Effective Diameter:	**1905.8 nm**
Polydispersity:	**0.292**
Avg. Count Rate:	**30.9 kcps**
Baseline Index:	**0.0**
Elapsed Time:	**00:10:00**

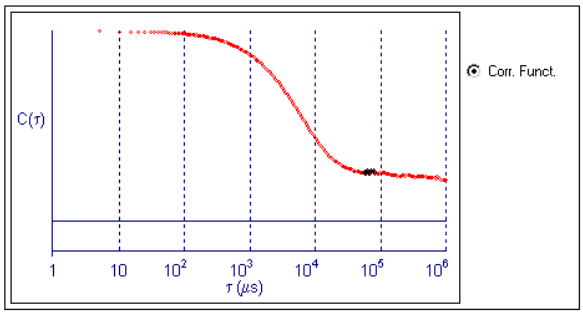

Run	Eff. Diam. (nm)	Half Width (nm)	Polydispersity	Baseline Index
1	2058.9	1120.7	0.296	0.0
2	1769.7	1068.6	0.365	0.0
3	1851.5	983.5	0.282	0.0
4	2006.8	1139.9	0.323	0.0
5	2205.8	959.7	0.189	0.0
6	1690.2	943.9	0.312	0.0
7	1734.9	936.1	0.291	0.0
8	1642.0	987.5	0.362	0.0
9	1575.9	864.6	0.301	0.0
10	1393.0	827.0	0.352	0.0
Mean	1792.9	983.2	0.307	0.0
Std. Error	77.1	32.2	0.016	0.0
Combined	1905.8	1029.9	0.292	0.0

FIGURE 20 Correlation Function for T52, First Wash

Sample ID	T-52M_1st wash_diluted #1A (Combined)
Operator ID	mertz
Elapsed Time	00:10:00
Mean Diam.	2623.0 nm
Rel. Var.	0.183
Skew	-0.536

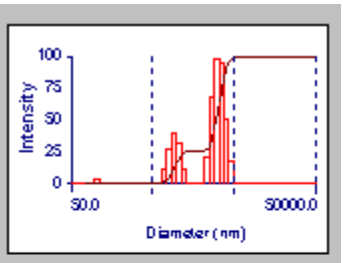

d(nm)	G(d)	C(d)	d(nm)	G(d)	C(d)	d(nm)	G(d)	C(d)
79.4	0	0	348.9	0	0	1533.4	0	26
90.8	0	0	399.2	0	0	1754.3	0	26
103.9	2	0	456.7	0	0	2007.0	0	26
118.9	0	0	522.5	0	0	2296.1	20	30
136.0	0	0	597.8	0	0	2626.8	69	44
155.6	0	0	683.9	11	3	3005.2	100	65
178.0	0	0	782.4	27	8	3438.1	96	86
203.7	0	0	895.1	40	17	3933.4	51	96
233.0	0	0	1024.0	32	23	4500.0	17	100
266.6	0	0	1171.5	10	26	5148.2	0	100
305.0	0	0	1340.3	0	26	5889.8	0	100

Intensity

FIGURE 21 Multisize Distribution for T52, First Wash

Sample ID	T-52M_2nd wash_diluted #2 (Combined)
Operator ID	mertz
Elapsed Time	00:10:00
Median Diam.	183.5 nm
Mean Diam.	206.2 nm
Polydispersity	0.264
GSD	1.622

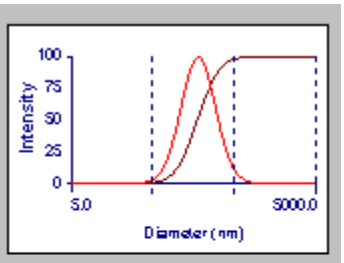

d(nm)	G(d)	C(d)	d(nm)	G(d)	C(d)	d(nm)	G(d)	C(d)
82.8	26	5	162.3	97	40	254.2	80	75
98.7	44	10	172.6	99	45	275.7	70	80
111.1	58	15	183.5	100	50	302.8	58	85
122.1	70	20	195.0	99	55	341.1	44	90
132.4	80	25	207.3	97	60	406.6	26	95
142.4	87	30	221.0	93	65			
152.3	93	35	236.4	87	70			

Intensity

Copy for Spreadsheet

FIGURE 22 Monomodal Size Distribution for T52, Second Wash

T-52M_2nd wash_diluted #2 (Combined)

Effective Diameter: 183.5 nm
Polydispersity: 0.264
Avg. Count Rate: 314.3 kcps
Baseline Index: 4.3
Elapsed Time: 00:10:00

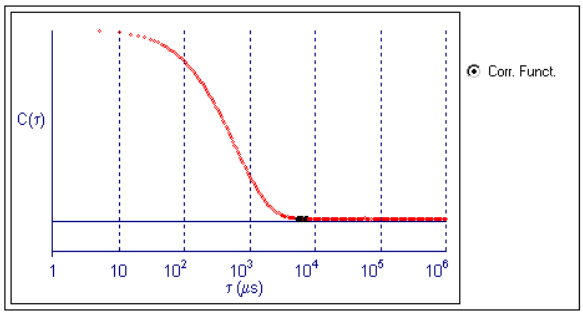

Run	Eff. Diam. (nm)	Half Width (nm)	Polydispersity	Baseline Index
1	193.4	99.0	0.262	9.1
2	181.8	91.4	0.253	8.4
3	176.8	85.2	0.232	8.3
4	169.9	88.7	0.273	5.6
5	175.4	90.0	0.263	9.5
6	183.3	98.5	0.289	9.8
7	183.3	91.8	0.251	4.3
8	188.7	99.9	0.280	9.5
9	185.3	92.8	0.251	5.8
10	188.3	97.8	0.270	9.3
Mean	182.6	93.5	0.262	8.0
Std. Error	2.2	1.6	0.005	0.6
Combined	183.5	94.2	0.264	4.3

FIGURE 23 Correlation Function for T52, Second Wash

Sample ID	T-52M_2nd wash_diluted #2 (Combined)
Operator ID	mertz
Elapsed Time	00:10:00
Mean Diam.	230.4 nm
Rel. Var.	0.110
Skew	-1.678

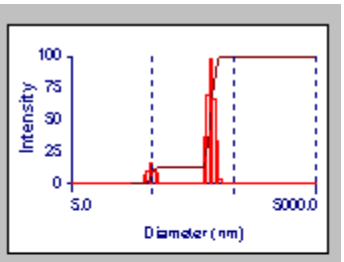

d(nm)	G(d)	C(d)	d(nm)	G(d)	C(d)	d(nm)	G(d)	C(d)
28.9	0	0	73.0	0	14	184.3	0	14
31.4	0	0	79.4	0	14	200.5	0	14
34.2	0	0	86.3	0	14	218.1	36	24
37.2	0	0	93.9	0	14	237.3	70	43
40.5	6	2	102.2	0	14	258.2	100	71
44.0	9	4	111.2	0	14	280.9	67	90
47.9	16	9	120.9	0	14	305.6	33	99
52.1	11	12	131.6	0	14	332.4	2	100
56.7	8	14	143.1	0	14	361.6	0	100
61.6	0	14	155.7	0	14	393.4	0	100
67.1	0	14	169.4	0	14	428.0	0	100

Intensity

FIGURE 24 Multisize Distribution for T52, Second Wash

Sample ID	T-5M_1st wash_diluted #3 (Combined)
Operator ID	mertz
Elapsed Time	00:09:00
Median Diam.	419.2 nm
Mean Diam.	463.5 nm
Polydispersity	0.223
GSD	1.566

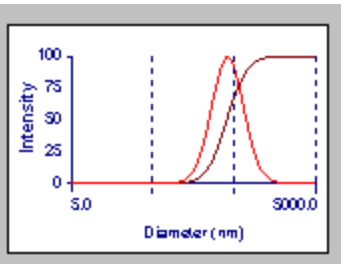

d(nm)	G(d)	C(d)	d(nm)	G(d)	C(d)	d(nm)	G(d)	C(d)
200.5	26	5	374.2	97	40	567.1	80	75
235.9	44	10	396.2	99	45	611.5	70	80
263.4	58	15	419.2	100	50	667.1	58	85
287.4	70	20	443.6	99	55	744.9	44	90
309.9	80	25	469.6	97	60	876.5	26	95
331.4	87	30	498.2	93	65			
352.7	93	35	530.2	87	70			

Intensity

Copy for Spreadsheet

FIGURE 25 Monomodal Size Distribution for T5M, First Wash

T-5M_1st wash_diluted #3 (Combined)

Effective Diameter: 419.2 nm
Polydispersity: 0.223
Avg. Count Rate: 263.0 kcps
Baseline Index: 5.1
Elapsed Time: 00:09:00

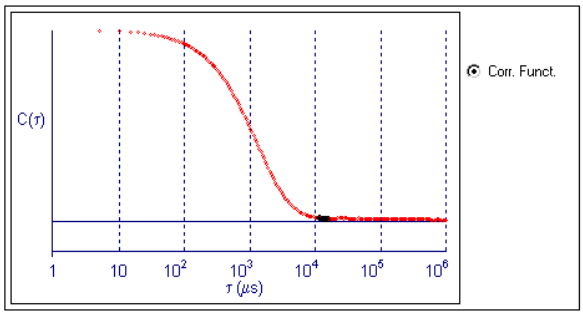

Run	Eff. Diam. (nm)	Half Width (nm)	Polydispersity	Baseline Index
1	441.2	232.5	0.278	3.4
2	424.0	176.4	0.173	5.6
3	425.8	212.1	0.248	7.2
4	418.3	193.2	0.213	3.9
5	418.8	194.7	0.216	0.1
6	412.8	205.1	0.247	5.0
7	411.8	177.6	0.186	4.5
8	423.7	198.5	0.219	9.3
9	411.5	216.8	0.278	8.8
10	406.8	164.8	0.164	1.9
Mean	419.5	197.5	0.223	5.5
Std. Error	3.5	7.3	0.014	0.8
Combined	419.2	197.8	0.223	5.1

FIGURE 26 Correlation Function for T5M, First Wash

Sample ID	T-5M_1st wash_diluted #3 (Combined)
Operator ID	mertz
Elapsed Time	00:09:00
Mean Diam.	555.1 nm
Rel. Var.	0.234
Skew	-0.173

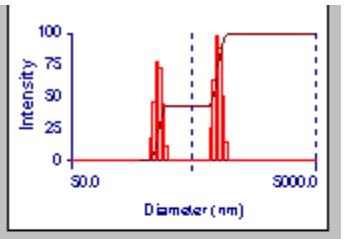

d(nm)	G(d)	C(d)	d(nm)	G(d)	C(d)	d(nm)	G(d)	C(d)
188.4	0	0	350.6	0	44	652.2	0	44
199.4	0	0	370.9	0	44	690.1	26	48
210.9	0	0	392.5	0	44	730.2	64	59
223.2	17	3	415.2	0	44	772.6	100	75
236.1	47	10	439.4	0	44	817.4	89	89
249.9	79	23	464.9	0	44	864.9	51	98
264.4	73	35	491.9	0	44	915.1	14	100
279.7	44	42	520.4	0	44	968.3	0	100
296.0	11	44	550.6	0	44	1024.5	0	100
313.1	0	44	582.6	0	44	1084.0	0	100
331.3	0	44	616.4	0	44	1146.9	0	100

Intensity

FIGURE 27 Multisize Distribution for T5M, First Wash

Sample ID	T-5M_2nd wash_diluted #4 (Combined)
Operator ID	mertz
Elapsed Time	00:07:00
Median Diam.	258.3 nm
Mean Diam.	280.7 nm
Polydispersity	0.181
GSD	1.503

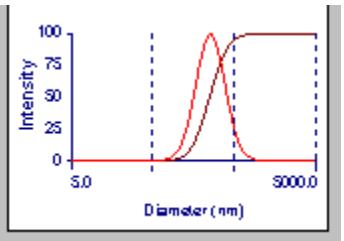

d(nm)	G(d)	C(d)	d(nm)	G(d)	C(d)	d(nm)	G(d)	C(d)
132.1	26	5	233.0	97	40	340.0	80	75
153.2	44	10	245.4	99	45	364.1	70	80
169.3	58	15	258.3	100	50	394.0	58	85
183.3	70	20	271.9	99	55	435.6	44	90
196.2	80	25	286.4	97	60	505.1	26	95
208.6	87	30	302.2	93	65			
220.8	93	35	319.8	87	70			

Intensity

Copy for Spreadsheet

FIGURE 28 Monomodal Size Distribution for T5M, Second Wash

T-5M_2nd wash_diluted #4 (Combined)

Effective Diameter: 258.3 nm
Polydispersity: 0.181
Avg. Count Rate: 285.2 kcps
Baseline Index: 7.6
Elapsed Time: 00:07:00

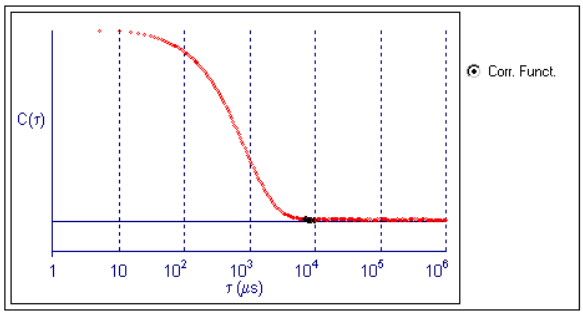

Run	Eff. Diam. (nm)	Half Width (nm)	Polydispersity	Baseline Index
1	267.0	125.2	0.220	7.8
2	256.7	97.0	0.143	2.8
3	259.2	104.7	0.163	7.3
4	259.2	123.7	0.228	8.1
5	252.5	100.5	0.158	2.8
6	251.4	106.0	0.178	8.6
7	259.7	93.8	0.130	9.0
8	252.1	72.4	0.082	5.0
9	257.3	116.5	0.205	8.1
10	254.8	104.0	0.167	9.4
Mean	258.4	110.5	0.184	8.3
Std. Error	1.8	4.4	0.013	0.3
Combined	258.3	109.8	0.181	7.6

FIGURE 29 Correlation Function for T5M, Second Wash

Sample ID	T-5M_2nd wash_diluted #4 (Combined)
Operator ID	mertz
Elapsed Time	00:07:00
Mean Diam.	324.1 nm
Rel. Var.	0.274
Skew	1.490

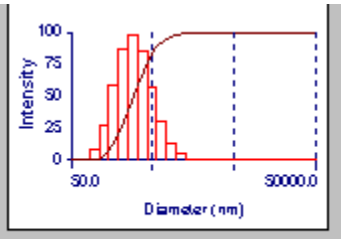

d(nm)	G(d)	C(d)	d(nm)	G(d)	C(d)	d(nm)	G(d)	C(d)
1.0	0	0	19.2	0	0	367.4	86	78
1.3	0	0	25.1	0	0	480.6	58	90
1.7	0	0	32.8	0	0	628.6	29	97
2.2	0	0	42.9	0	0	822.2	12	99
2.9	0	0	56.1	0	0	1075.4	4	100
3.8	0	0	73.4	0	0	1406.6	0	100
5.0	0	0	96.0	7	2	1839.8	0	100
6.5	0	0	125.5	27	7	2406.4	0	100
8.6	0	0	164.2	59	20	3147.5	0	100
11.2	0	0	214.8	89	39	4116.8	0	100
14.7	0	0	280.9	100	60	5384.7	0	100

Intensity

FIGURE 30 Multisize Distribution for T5M, Second Wash

9.3 EXPERIMENT

Samples were obtained by hand shaking the sorbents with 0.1 M HNO_3 for 1 minute.

The DLS apparatus consisted of a modified 4700c photon correlation spectrometer from Malvern Instruments Ltd. The system has a uniphase (variable power output of 3 to 75 mW) argon ion laser. The sample cell rests in the sample chamber in a temperature-controlled, filtered water bath. All optical components of the system are mounted on an enclosed optical table (see Figure 1). The correlator records the scattering intensity from small scattering volumes in time intervals as short as 50 ns. The particle sizing data are analyzed by using the commercial software supplied with the unit, which consists of well-accepted methods: cumulants and CONTIN. The particle size is calibrated on the entire system as a whole using National Institute of Standards and Technology (NIST) polystyrene latex standards (nominal sizes of 100 and 300 nm).

10 ALUMINA SOLUBILITY

The solubility of alumina was modeled by using the thermochemical modeling code OLI-ESP (OLI Systems Inc, ESP Revision 7.0.55, thermodynamic database: PUBLIC, 2001). The results indicated that alumina might be meta-stable in dilute nitric acid, and based on equilibrium thermodynamics, it is predicted to be soluble at a pH of 1 (Figure 31). However, the kinetics of dissolution are probably very slow and/or require an activation energy. It is not uncommon for Al(III) to contain solids such as aluminum silicates, which are predicted to be soluble in groundwater yet persist in rock aquifers.

Solubility profiles for alumina were also calculated by using ChemEQL software (Carrier et al. 2007; see Figure 32). Similarly, alumina appears metastable under acidic conditions. Moreover, Carrier et al. (2007) demonstrated that at a pH over 4, after a 10-h contact, the alumina suspension dissolved, leading to a supersaturated solution from which aluminum hydroxide particles precipitated and grew independently from the alumina surface. Thermodynamically stable gibbsite particles were formed in the acidic range, while bayerite became the predominant phase at a nearly neutral pH. The relevance of this phenomenon with regard to MIPS conditions requires further study.

Our studies showed that the solubility of alumina sorbents was three orders of magnitude higher than the solubility of titania-based sorbents (Table 10). The differences in the solubilities of alumina samples from different suppliers reflected the uniformity of particle size. For example, alumina from Sigma-Aldrich was not of sorbent quality and contained a large amount of fines (Figure 33), whereas the AG4 sample from BioRad (Figure 34) had a much narrower particle size distribution, which was reflected in its lower solubility. BioRad does not

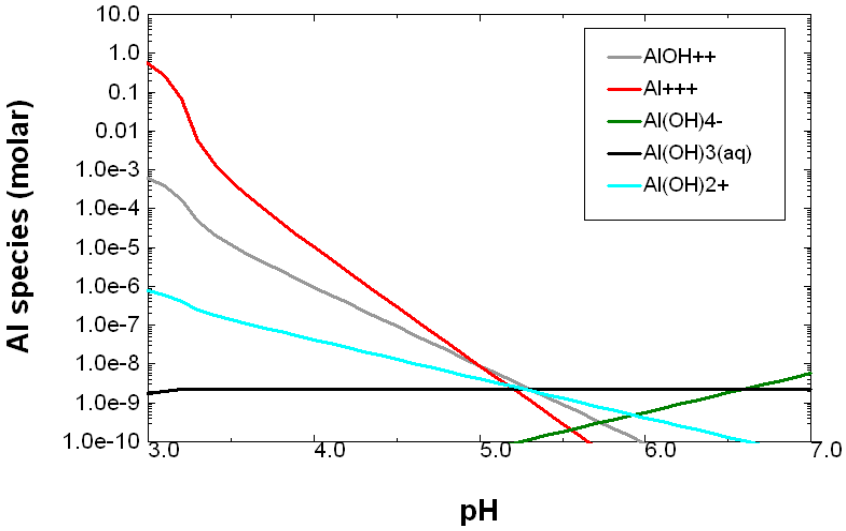

FIGURE 31 Solubility of Alumina as Function of pH Modeled by Using OLI-ESP Code

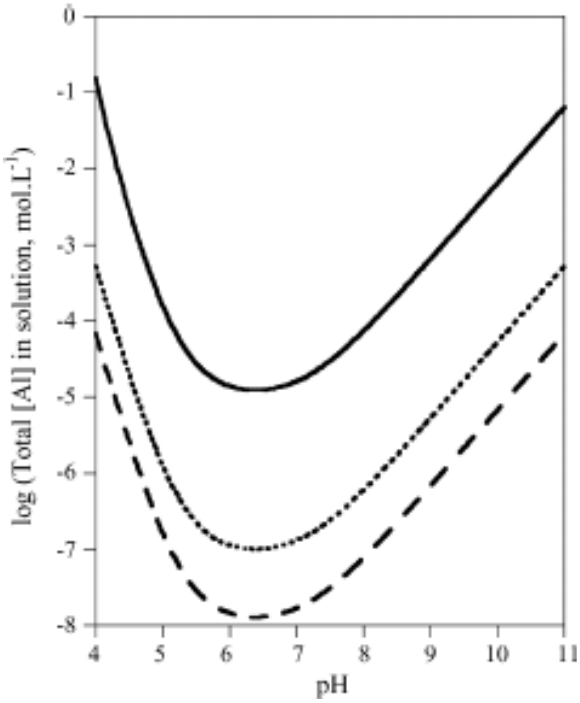

FIGURE 32 Solubility Profiles [Concentration of Al(III) in solution as a function of pH for γ-Al_2O_3 (solid line), bayerite (dotted line), and gibbsite (dashed line)] (Carrier et al. 2007)

TABLE 10 ICP-MS Results of Alumina Solubility in 0.1 M HNO_3

	Solubility of Alumina (ppm)						
	Sorbent Technologies		Dynamic Adsorbents				
Conditions	Act. I (50–200 μm)	Super Act. I (50–200 μm)	Alumina R (50–200 μm)	Act. I (50–200 μm)	Super Act. I (50–200 μm)	BioRad AG4 (150 mesh)	Sigma Aldrich Act. I (150 mesh)
RT, 6 days, 0.1 M HNO_3	200	213	157	109	142	93.2	436
60°C, 24 h, 0.1 M HNO_3	278	334	245	222	195	181	415

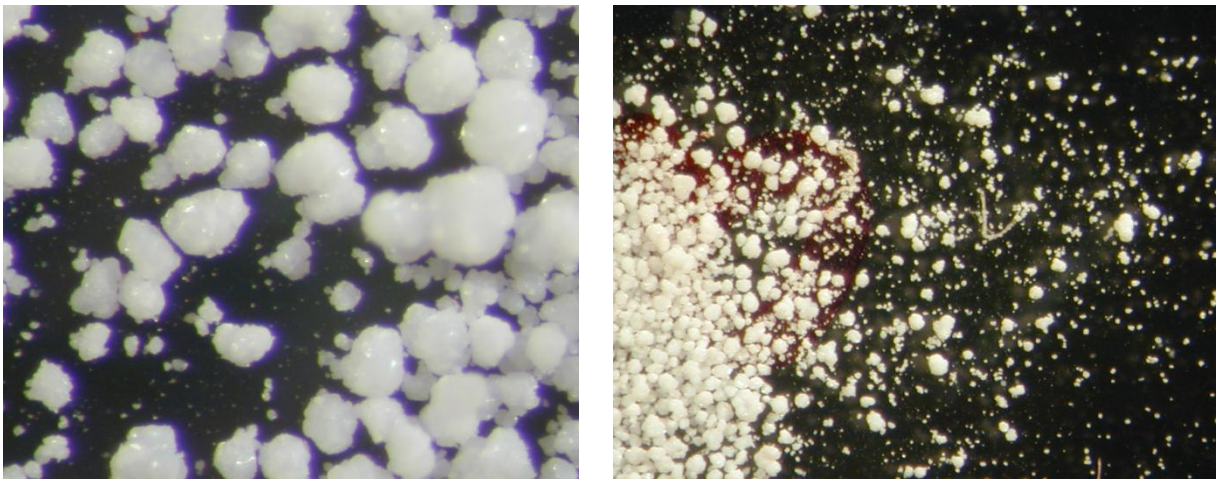

FIGURE 33 Images of Alumina Sample Act. I from Sigma Aldrich, 150 Mesh

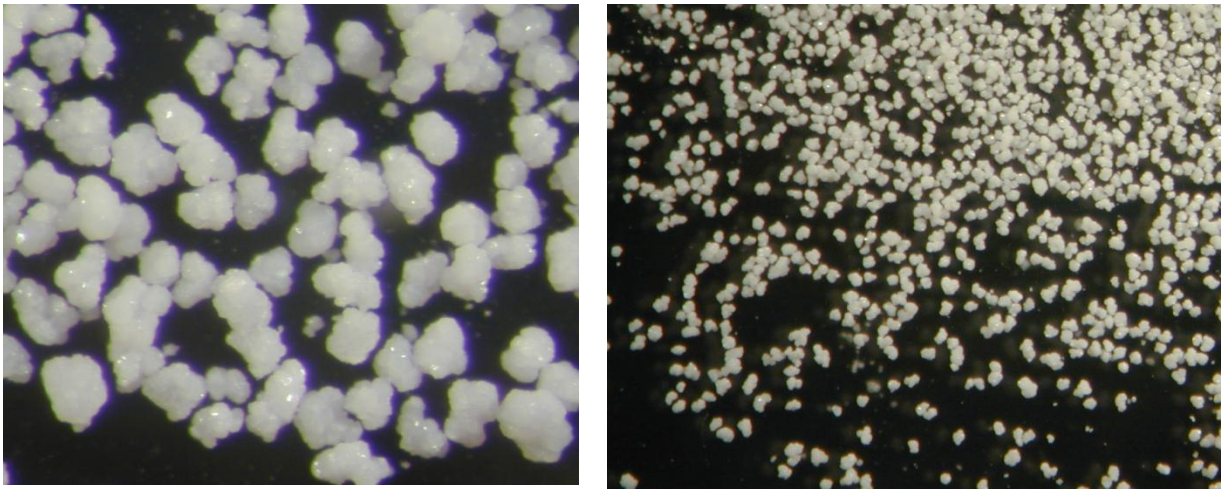

FIGURE 34 Images of Alumina Sample AG4 from BioRad, 150 Mesh

manufacture AG4 anymore. However, two other manufacturers of sorbent-quality alumina were identified: Sorbent Technologies and Dynamic Adsorbents. Samples were obtained from them.

A narrow particle-size distribution and a minimal amount of fines in the sorbent are important factors with regard to back pressure concerns. It is anticipated that an alumina column would have a substantial bed height due to its low Mo K_d values and subsequent long mass transfer zone. Therefore, a uniform particle size would allow a long column to be designed without exceeding back pressure limits.

The impact of high concentrations of Al^{3+} on the speciation and solubility of other components of the reactor solution should be investigated if alumina continues to be a candidate for MIPS. In addition, the behavior of an aluminum supersaturated solution and the possibility of aluminum-hydroxide precipitation and independent particle growth should be investigated.

11 Mo STRIPPING

11.1 INTRODUCTION

Small columns were prepared to investigate the stripping of Mo from T5M-, T52-, S80-, and AG4-packed columns by using 1 M NaOH to elute Mo. The results in Table 11 indicate that Mo recovery can be greater than 95% for T5M, T52, and S80. Product recovery from AG4 was about 90%. These results will be repeated in the future to achieve a more accurate product recovery. Figure 35 shows the elution of Mo from T5M-, T52-, S80-, and AG4-packed columns and indicates that Mo can be eluted within four bed volumes for all sorbents.

TABLE 11 Percent Recovery of Mo-99 from T5M, T52, S80, and AG4

Mo Recovery	T5M	T52	S80	Alumina
Total % recovery[a]	97 ± 5	93 ± 5	100 ± 5	88 ± 5

[a] Includes 5 mL of 0.1 M HNO_3 washes.

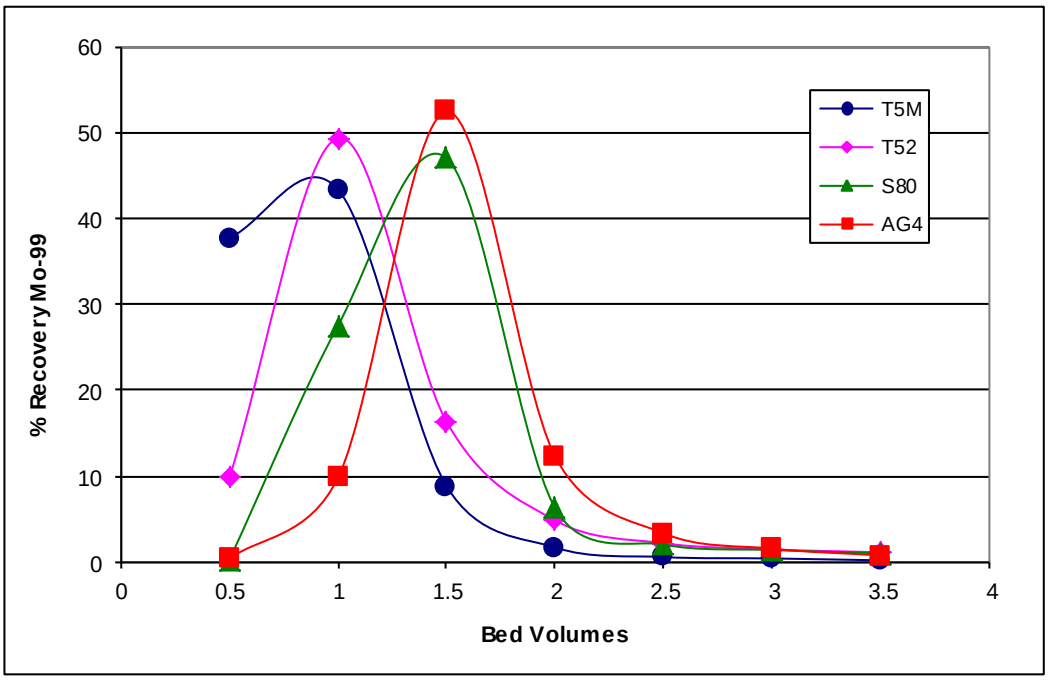

FIGURE 35 Percent Recovery of Mo-99 as a Function of the Number of Bed Volumes

11.2 EXPERIMENT

Columns were packed with 2 mL of T5M, T52, S80, and AG4 sorbents, pre-equilibrated with 0.1 M HNO_3, and loaded with 50 μL of 10 ppm Mo in 0.1 M HNO_3 solution spiked with ^{99}Mo. The columns were then washed with 5 × 1 mL of 0.1 M HNO_3 followed by 7 × 1 mL of 1 M NaOH. Recovery of Mo was calculated from counting the starting Mo solution and the individually collected fractions on a NaI gamma counter.

12 UPTAKE OF COMPETING COMPONENTS

The uptake of competing components was measured by contacting T5M and T52 (1 g) with 10 mL of a simulated fuel solution at pH 1, without uranium, for 24 h at 55°C (Table 12). The composition of the fuel solution was based on ORIGEN calculations for 90-days burnup for an AHR fuel solution (Neally 2008). The following components of the fuel solution were analyzed by using ICP-MS: Fe, Se, Rb, Sr, Y, Mo, Ru, Rh, Ag, Cd, Sn, Cs, Ba, La, Ce, Nd, Sm, Eu, and Gd. Ion chromatography was used to analyze I^-. The components that exhibited K_d values above 10 for T52 were Fe (42), Ru (88), Se (≥49), and Rh (14). For T5M K_d, Se was ≥49, and Ru was 44. I^- had K_d values of 1 and 6, respectively, for T52 and T5M.

The uptake of competing components was also measured for S80 and AG4 under similar conditions (Table 12). The following components of the fuel solution were analyzed by ICP-MS: Fe, Se, Rb, Sr, Y, Zr, Mo, Ru, Ag, Cd, Sn, Te, Cs, Ba, La, Ce, Nd, Sm, Eu, and Gd. The components that exhibited K_d values above 10 for S80 were Se (≥349), Zr (60), Ag, (147) Sn (18), and Te (≥4,373). For AG4 K_d, Se was ≥349, Ag was 24, Sn was 48, and Te was ≥4,373. Rh, which was present as perrhenate anion at pH 1, was not analyzed for uptake by S80 and AG4, but it likely would have exhibited K_d values above 10.

TABLE 12 Uptake of Ions from a Simulated Fuel Solution in the Absence of Uranium

	Sorbent K_d values			
Element	T52	T5M	TiO_2 sorbent	Alumina
Fe	42	9	5	0
Se	≥49	≥49	≥ 349	≥ 349
Rb	0.1	0.0	0	0
Sr	0.0	0.0	0	0
Y	0.7	0.1	0	0
Mo	≥2599	137	≥3110	≥3110
Ru	88	44	3	1
Rh	14	3	-	-
Ag	0.0	0.0	147	24
Cd	2	0.5	0	0
Sn	0.0	4.8	18	49
Cs	0.2	0.0	0	0
Ba	0.1	0.0	0	0
La	0.1	0.0	0	0
Ce	0.2	0.0	0	0
Nd	0.2	0.0	0	0
Sm	0.9	0.2	0	0
Eu	0.9	0.2	0	0
Gd	1	0.3	0	0
I	1	6	-	-
Zr	-	-	60	9
Te	-	-	≥4373	≥4373

13 COLUMN SIZE

The amount of sorbent needed to design a column for MIPs Using S80, AG4, T5M (200–400 μm) and T52 (200–400 μm) was calculated by using data obtained at 1.4 M NO_3^- and a pH of 1 (Chung and Wang 2009). The amount of sorbent for a column with a 10-cm inside diameter and a linear velocity of 21 cm/min was 0.2 kg and 0.3 kg, respectively, for S80 and AG4, and 1.3 kg and 1.9 kg, respectively, for T5M and T52 (Table 13). The calculated amounts of sorbent needed to design a column is expected to change once the presence of uranium in the solution is included in the calculations. In the presence of 150 g-U/L, Mo K_d values for S80, T52, and T5M decreased about one order of magnitude. However, in the presence of uranium, Mo K_d values for AG4 decreased by about two orders of magnitude, resulting in a Mo K_d value of 270. Also, these calculations indicate that a column designed using T5M would be about 30% smaller than a column containing T52. However, experiments carried out in the presence of uranium have consistently shown that in the presence of uranium, T52 has higher K_d values. Therefore, it is expected that a column designed using T52 would be smaller than a column with T5M under MIPS conditions.

TABLE 13 Recommended Column Designs Based on Pressure Drop Constraints and Mass Transfer Zone Calculations (60°C, pH 1, and *DV* = 4% *CV*)

Sorbent	$d_{p,\,avg}$ (μm)	$[NO_3^-]$ (N)	*ID* (cm)	u_s (cm/min)	L_{max} (cm) at 0.8 atm	L_{min} (cm)	L_{min}/ID	CV_{min} (L)	$W_{sorbent,\,min}$ (kg)	Δ*P* for L_{min} (atm)
S	80	1.4	10	21	16	2	0.2	0.2	0.2	0.10
		2	10	21	12	5	0.5	0.4	0.6	0.33
Al	112	1.4	10	21	27	4	0.4	0.2	0.3	0.12
T5M	300	1.4	10	21	186	15	1.6	1.2	1.3	0.07
		2	10	21	165	20	2	1.6	2.5	0.1
T52	300	1.4	10	21	114	16	1.6	1.3	1.9	0.1
T5M	700	1.4	10	21	968	67	6.7	5.3	5.8	0.06
		2	10	21	860	80	8	6.3	10	0.07
T52	700	1.4	10	21	594	80	8	6.3	9.4	0.1

14 FUTURE WORK

14.1 LANGMUIR ISOTHERM DATA IN THE PRESENCE OF 150 g-U/L, pH 1, 60°C

Uranium has a major effect on the sorption of Mo by S80, T52, T5M, and AG4. This effect cannot be simply accounted for by the aqueous equilibrium of uranyl molybdate, since the presence of uranium has varying effects on the K_d values of different sorbents, most likely related to the different sorption mechanisms and/or the populations of different sorption sites on the sorbents. Therefore, Langmuir isotherm data will be obtained for S80, T52, and alumina sorbents in the presence of 150 g-U/L.

14.2 PRESENCE OF NANOPARTICLES IN THE REACTOR SOLUTION

Nanoparticles in the reactor solution can originate from the mechanical degradation of the sorbent and/or from the precipitation of the aluminum hydroxide or titanium hydroxide saturated solution. Further work will be carried out to increase our understanding of the formation of nanoparticles or precipitates in the reactor solution and of ways to efficiently remove them.

14.3 MECHANICAL STABILITY OF THE SORBENTS

The mechanical stability of the sorbents and its effect on the column backpressure will be investigated. Packed column testing will be done to measure backpressure versus time for long-duration tests in which the flow rate and feed composition will be varied from one test to the next. The effects of these long-duration tests on the physical and chemical properties of the sorbents will also be measured.

14.4 ALUMINUM HYDROXIDE

The effect of the concentration (in ppm) of aluminum hydroxide in the reactor solution should be included in the modeling studies to achieve an understanding regarding the possibility of precipitate formation in the reactor solution.

14.5 WASHING OF URANYL NITRATE FROM S80 PACKED COLUMN

It is not clear at this point if it would be more practical to wash S80 with a large amount of 0.1 M HNO_3 (20 to 30 bed volumes) or to use 1 M HNO_3. The concern associated with using 0.1 M is whether a large volume of solution could be recycled back into the reactor. The concerns associated with using 1 M are the loss of Mo (1.5% in a batch experiment for 24 h at 60°C), the solubility of S80 at a pH of 0, and the degradation of MIPS separation equipment at a pH of 0. The loss of Mo when the sorbent is scrubbed with 1 M HNO_3 will be validated in a

column mode. The solubility of S80 in 1 M HNO_3 will be determined experimentally, and the corrosion of the Mo recovery system at a pH of 0 will be determined.

14.6 Mo RECOVERY

It is clear that Mo can be recovered from S80, T52, T5M, and AG4 with ≥90% efficiency. Attempts to measure Mo recovery with greater accuracy have provided inconsistent results. These measurements will be carried out again in a small column mode, or radiometrically when Mo-99 becomes available. We have found a source, and, if all goes well, these tests can resume in early August 2009.

15 REFERENCES

Beasley, H., 2007, "SEM Report," for W.A. McInteer, BWXT Services, Inc., Lynchburg, Va., Sept. 20.

Brunauer, S., 1938, "Adsorption of Gases in Multimolecular Layers," *J. Am. Chem. Soc.* 60:309–319.

Carrier, X., et al.,, 2007, " Transformations of Gamma-Alumina in Aqueous Suspensions 1. Alumina Chemical Weathering Studied as a Function of pH," *J. Coll, Inter. Sci.* 308:429–437.

Chung, P.-L., and N.-H. L. Wang, 2009, *Design, Scale up, and Optimization of Column Processes for the Recovery of a Medical Isotope,* Progress Report, Part II, Purdue University, Lafayette, Ind., July.

Diebold, U., 2003, "The Surface Science of Titanium Dioxide," *Surface Science Reports* 48:53–229.

Fortner, J., 2008, unpublished information, Argonne National Laboratory, Argonne, Ill., March.

Hiskey, C.F., and V.W. Meloche, 1940, "The Nature of the Thiocyanate Complex of Molybdenum," *J. Am. Chem. Soc.* 62(6):1565–1574.

Neally, G., 2008, "ORIGEN Calculations for 90 Days Burnup for an AHR Fuel Solution," BWXT Services, Inc., Lynchburg, Va., Feb.

Sugimoto, T., et al., 2002, "Synthesis of Uniform Anatase TiOx Nanoparticles by Gel-Sol Method. 1. Solution Chemistry of Ti(OH)(4-n)+(n) Complexes," *J. Colloid Interface Sci.* 252(2):339–346.

Vandegrift, G., et al., 2008, unpublished information, Argonne National Laboratory, Argonne, Ill., March.

Vissenberg, M.J., et al., 2000, "Tungstate Versus Molybdate Adsorption on Oxidic Surfaces: A Chemical Approach," *J. Phys. Chem. B* 104:8456–8461.

Weast, R.C., et al. (editors), 1964, "Physical Constants of Inorganic Compounds," in *Handbook of Chemistry and Physics,* 46th edition, The Chemical Rubber Co., Cleveland, Ohio.

Winkler, J., S., et al.,1999, *Titanium Dioxide — Properties and Applications in LC,* Sachtleben.

Yebka, B., et al., 1999, "Electrochemical Behavior of Hydrated Molybdenum Oxides in Rechargeable Lithium Batteries," *Ionics* 5(3–4):236–243.

Chemical Science and Engineering Division
Argonne National Laboratory
9700 South Cass Avenue, Bldg. 205
Argonne, IL 60439-4837

www.anl.gov

Argonne National Laboratory is a U.S. Department of Energy
laboratory managed by UChicago Argonne, LLC